Review

Emerging Layered Materials and Their Applications in the Corrosion Protection of Metals and Alloys

Ramaraj Sukanya [1], Tara N. Barwa [1], Yiran Luo [1], Eithne Dempsey [1,2] and Carmel B. Breslin [1,2,*]

1   Department of Chemistry, Maynooth University, W23 F2H6 Maynooth, Co. Kildare, Ireland;
    sukanyaram33@gmail.com (R.S.); tara.barwa.2023@mumail.ie (T.N.B.); yiran.luo.2023@mumail.ie (Y.L.);
    eithne.dempsey@mu.ie (E.D.)
2   Kathleen Lonsdale Institute for Human Health Research, Maynooth University,
    W23 F2H6 Maynooth, Co. Kildare, Ireland
*   Correspondence: carmel.breslin@mu.ie

Abstract: Metals and alloys are essential in modern society, and are used in our daily activities. However, they are prone to corrosion, with the conversion of the metal/alloy to its more thermodynamically-favored oxide/hydroxide phase. These undesirable corrosion reactions can lead to the failure of metallic components. Consequently, corrosion-protective technologies are now more important than ever, as it is essential to reduce the waste of valuable resources. In this review, we consider the role of emerging 2D materials and layered materials in the development of a corrosion protection strategy. In particular, we focus on the materials beyond graphene, and consider the role of transition metal dichalcogenides, such as MoS_2, MXenes, layered double hydroxides, hexagonal boron nitride and graphitic carbon nitride in the formulation of effective and protective films and coatings. Following a short introduction to the synthesis and exfoliation of the layered materials, their role in corrosion protection is described and discussed. Finally, we discuss the future applications of these 2D materials in corrosion protection.

1. Introduction

Metals and alloys are essential in modern society, and depending on their properties, they are used in a multitude of applications. For example, aluminum and titanium are lightweight and find applications in the aerospace industry [1], while copper or electroplated copper is typically employed in electronic applications [2], and steels are used in construction and transportation [3]. Although advances have been made in the processing of metals and alloys, leading to improvements in their performance, metals and alloys are prone to corrosion [4]. This is a natural process that converts the pure metal or alloy, when in contact with its environment, into its thermodynamically-favored oxide, hydroxide, carbonate or sulfide. As a result, there is gradual deterioration and destruction of the material, which can eventually lead to a loss in function, structural failure, or indeed environmental contamination with the release of hazardous metal ions. Additional metals or alloys are often employed to replace the failed component, and this has implications for sustainability with an over-utilization of natural resources [5]. Sustainability is an essential consideration in the modern world. Accordingly, innovative corrosion-protection strategies are required to minimize the premature repair or replacement of metals and alloys.

The corrosion reaction can be described as two half-cell reactions, as illustrated in Equations (1) and (2), or in Equations (1) and (3), where Me represents a metal or alloy in an aqueous media or with a layer of adsorbed water molecules, which is relevant in atmospheric corrosion. The conversion of Me to Me^{n+} corresponds to the oxidation half reaction, while the accompanying reduction half reaction may involve either the reduction

of dissolved $O_2(g)$, as seen in Equation (2), or the reduction of $H^+(aq)$, which becomes the favored reaction under acidic conditions. As these reactions proceed, different forms of corrosion emerge, including more general dissolution, or localized forms of corrosion, such as pitting [4,6], crevice, intergranular or galvanic corrosion [7]. Another form that can traced to the environment in which Me functions includes stress corrosion [7].

$$Me \rightarrow Me^{n+} + ne^- \tag{1}$$

$$O_2(g) + 4H^+(aq) + 4e^- \rightarrow 2H_2O(aq) \tag{2}$$

$$2H^+(aq) + 2e^- \rightarrow H_2(g) \tag{3}$$
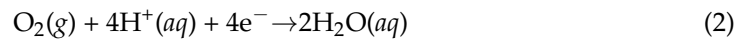
In order to protect Me from corrosion, the transfer of electrons must be impeded or eliminated by inhibiting the oxidation half, reduction half or both half reactions. For many years, hexavalent chromium (Cr(VI)) was used as a very effective corrosion inhibitor [8], but with its high levels of toxicity to both humans and aquatic life, it is no longer an option in the design of corrosion-protective coatings or technologies [9]. Consequently, alternative approaches are required, and various surface modifications and protective coatings have been formulated, ranging from polymeric coatings [10,11] and conversion coatings [12] to the employment of more recent materials, such as metal organic frameworks (MOFs) [13], all aimed at preventing or reducing the rate of corrosion [14,15].

Since the discovery of graphene, a host of new 2D materials has been uncovered or rediscovered, and these materials, with their intriguing properties, are finding applications in different sectors, ranging from energy [16,17] and sensors [18] to biomedical applications [19]. It is no surprise that they are also emerging as suitable materials for the corrosion protection of metals and alloys. Among the various 2D materials that have attracted attention in the formulation of corrosion protection strategies, graphene is one of the most widely considered [20,21]. However, the long-term corrosion-protective capacity of graphene is not always satisfactory [22], and there are a number of good reviews already available in the literature that describe the performance and limitations of graphene in the development of a corrosion-control technology [23,24].

Accordingly, in this review, we focus on other families of emerging layered and 2D materials, and these include transition metal dichalcogenides (TMDs), layered hexagonal boron nitride (h-BN), graphitic carbon nitride (g-C_3N_4), MXenes and finally the more established layered double hydroxides (LDHs), as illustrated in Figure 1. Initially, we briefly introduce these materials and describe some of the most common methods employed in their synthesis. Next, we review and discuss the corrosion-protective properties of the selected 2D materials. Finally, the challenges that remain to be resolved before these 2D materials can be employed in the design of a corrosion protection technology are highlighted and discussed.
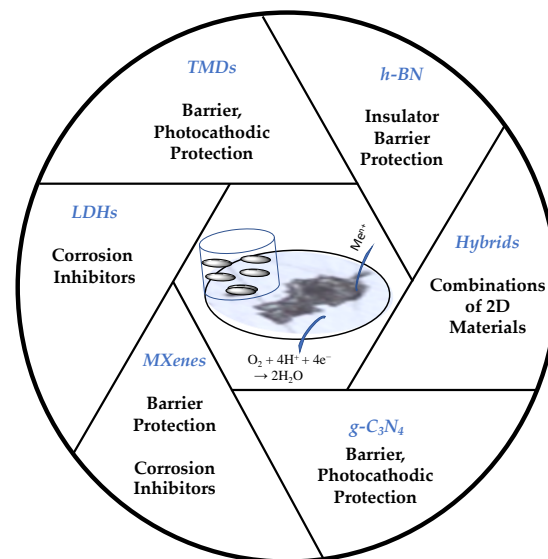
Figure 1. Schematic of the 2D materials and their primary roles in corrosion protection.

2. Layered Materials and Their Fabrication Methods

In Figure 2, schematic representations of layered LDHs [25], TMDs [26], MXenes [27], h-BN [28] and g-C_3N_4 [29] are presented. This highlights the layered assemblies that exist with different elements or combinations of elements. In these layered structures, van der Waals forces exist between the adjacent layers, and these control the interlayer distance and stacking modes. The LDHs (Figure 2A), are a family of ionic layered double hydroxides, and can be represented as $\left[M_{1-x}^{2+} M_x^{3+} (OH)_2 \right]^{q+} (A^{n-})_{q/n} \cdot yH_2O$, where M is a cation and A represents an anion [30]. The divalent cationic species are commonly Mg^{2+}, Zn^{2+}, Fe^{2+} or Ni^{2+}, while the trivalent cations are typically Al^{3+} or Fe^{3+}. Charge compensation of the divalent and trivalent cations is achieved with anions, A^{n-}, and these can include CO_3^{2-}, Cl^-, SO_4^{2-} and RCO_2^-. Clearly, LDHs have interesting characteristics in terms of the formulation of a corrosion control technology, as corrosion inhibitors can be easily introduced as the A species [31]. In the literature, LDHs are normally represented as M-M-LDH (e.g., Mg-Al-LDH) and this notation is also used in this review.

The TMDs can be represented as MX_2, where M is a transition metal such as Mo or W, and X represents the chalcogen atoms, S, Se or Te [32]. The M atoms are sandwiched between two chalcogen atoms to give X–M–X. The most widely studied TMD is MoS_2, which is finding applications in a diverse range of sectors, including energy [33] and sensors [34]. The layers are stacked and held by weak van der Waals forces, as illustrated in Figure 2B, while covalent bonding exists between the M and X atoms. The TMDs can exhibit different crystal phases, with the two main phases being the octahedral coordination phase (1T), which exhibits metallic-like properties, and the trigonal prismatic phase (2H), which has semiconductor-like characteristics.

MXenes are another interesting family of 2D materials, and comprise metal carbides or nitrides [35,36]. These are derived from their parent MAX phase, which has a 3D structure, as illustrated in Figure 2C. The MAX phases are denoted as $M_{n+1}AX_n$, where M represents an early transition element, such as Ti; A corresponds to a Group 13 or 14 element, usually Al; and X is carbon or nitrogen [35]. The *n* is an integer, and can adopt values ranging from 1 to 3. The MAX phases adopt a typical solid structure, but once the Al layer is etched and removed, the resulting layers are stacked in a hexagonal lattice, as shown in Figure 2C, where the characteristic accordion morphology is evident. The MXenes can be formed by the selective etching of the A element, as the bonding between M-A is generally weaker than between M-X [37].
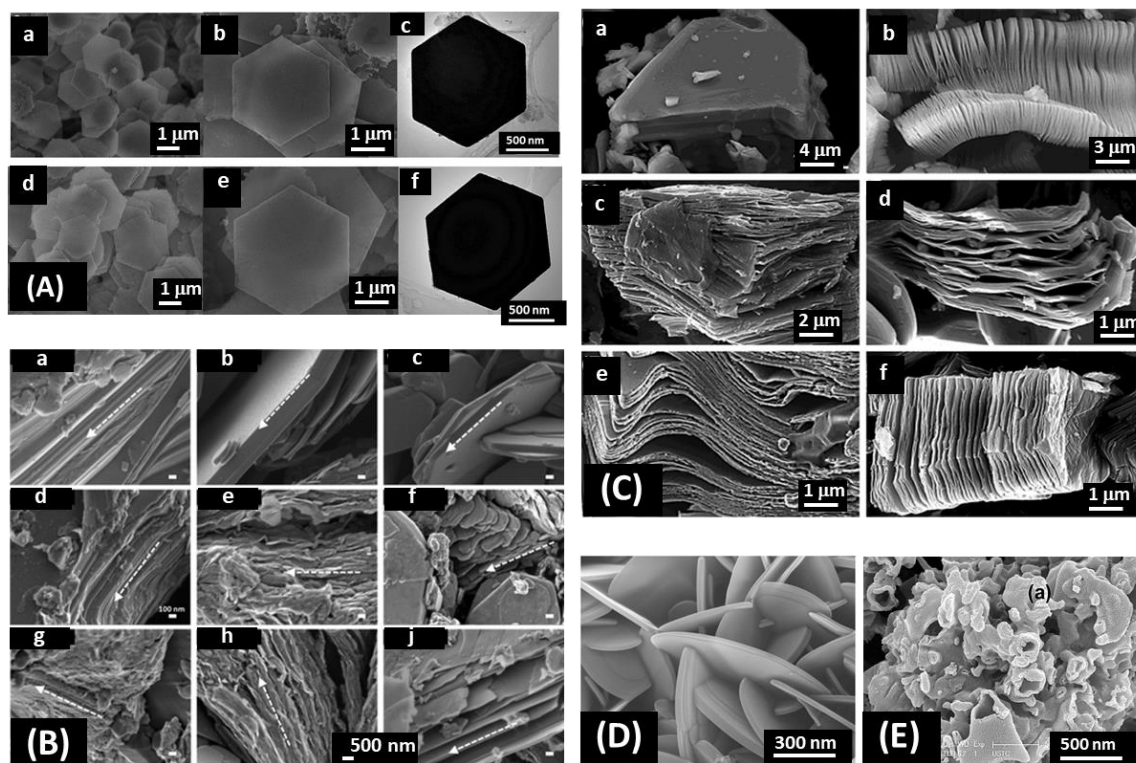
Figure 2. Micrographs of (**A**) LDHs. (**a**,**b**) SEM micrographs of I⁻-intercalated Co−Fe-LDHs, (**c**) TEM image of I⁻-intercalated Co-Fe-LDHs, (**d**,**e**) SEM images of ClO_4^--intercalated LDHs, and (**f**) TEM image of ClO_4^--intercalated LDHs.Adapted with permission from Renzhi et al. [25], copyright American Chemical Society, 2007. (**B**) Bulk TMDs. (**a**) $MoSe_2$ (**b**) WS_2 and (**c**) WSe_2, following treatment with methyllithium; (**d**) $MoSe_2$, (**e**) WS_2, and (**f**) WSe_2, and following treatment with butyllithium; (**g**) $MoSe_2$, (**h**) WS_2, and (**j**) WSe_2. Adapted with permission from Eng et al. [26], copyright American Chemical Society, 2014. (**C**) MXenes. (**a**) Ti_3AlC_2 MAX phase, (**b**) Ti_3AlC_2, (**c**) Ti_2AlC, (**d**) Ta_4AlC_3, (**e**) $TiNbAlC$, and (**f**) Ti_3AlCN after HF treatment. Adapted with permission from Naguib et al. [27], copyright American Chemical Society, 2012. (**D**) h-BN, FE-SEM images of h-BN nanosheets prepared at 1200 °C. Adapted with permission from Rui et al. [28], copyright American Chemical Society, 2009. (**E**) $g-C_3N_4$ synthesized from urea. Adapted with permission from Dong et al. [29], copyright Elsevier, 2013.

Graphitic carbon nitride ($g-C_3N_4$) [38] and h-BN [39] have similarities with graphene, and are often considered as analogues of graphene. Consequently, these are interesting materials in terms of corrosion protection as they can potentially provide a barrier to diffusion, in a manner similar to that seen with graphene. The layered h-BN, shown in Figure 2D, has alternating boron and nitrogen atoms in a honeycomb structure [39]. The 2D monolayer h-BN is considered analogous to graphene, however with a bandgap energy of approximately 5.9 eV, it is an insulator [40]. Again, weak van der Waals interactions exist between the h-BN planes. Likewise, $g-C_3N_4$ is considered an analogue of graphite [38]. It has a stacked structure consisting of π-conjugated graphitic planes formed through sp^2 hybridization of the C and N atoms. There are two structural isomers of $g-C_3N_4$, a melamine-based arrangement comprising condensed s-triazine units with rings of C_3N_3, and a tri-*s*-triazine subunit with rings of C_6N_7 connected through tertiary amino groups [41]. The tri-*s*-triazine unit is more thermodynamically stable and is widely accepted as the basic unit in the formation of the $g-C_3N_4$ network [42].
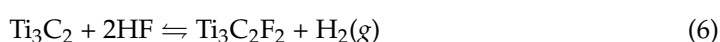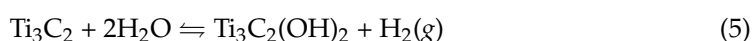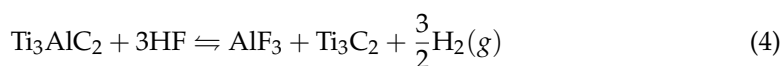
These 2D materials can be synthesized either by a top-down approach (mechanical or solution exfoliation of the bulk material) [43,44] or by bottom-up growth (chemical vapor deposition, pulsed laser deposition, or various vapor phase deposition methods) [45,46]. In terms of scalability, large-scale manufacturing and relevance to corrosion protection

technologies, the top-down approaches are more applicable. Although the epitaxy-based methods can be employed to produce defect-free monolayers with high crystallinity, they are very sensitive to the substrates, and require specific orientations. The first step in the top-down approach is the production of the parent bulk material, which is then followed by an exfoliation step. The methodologies employed in the synthesis of the bulk materials are summarized in Table 1, where it is evident that the parent LDHs and TMDs are relatively easily formed using hydrothermal synthesis [47,48]. In contrast, g-C_3N_4 is formed through the pyrolysis of nitrogen-rich precursors [49]. High-temperature processing, and in many cases high pressures, are required in the preparation of bulk h-BN [50,51] and the MAX phases are formed by sintering processes [52].

Table 1. Summary of the main synthesis methods used to form the 2D materials.

Methodology	Bulk Material	Details
hydrothermal/ solvothermal synthesis	TMDs LDHs	Relatively low temperatures, 100–200 °C, short processing times, economic, and an environmentally acceptable water-based synthesis (hydrothermal). Addition of organic solvents (solvothermal) can be used to tune the properties of the final product, including shape and size. Overall, efficient, fast and simple approach.
co-precipitation solution-based reactions	LDHs	Simple solution-based reactions, involving precursor salts of the LDH cations and anions, can be carried out at room temperature or at slightly elevated temperatures.
high temperatures and/or pressures	h-BN	Temperatures in the vicinity of 1300° to 1800 °C are employed.
sintering methods	MAX phases	Temperatures in the vicinity of 1100° to 1500 °C are employed.
pyrolysis and polycondensation	g-C_3N_4	Pyrolysis of nitrogen-rich precursors, followed by polycondensation; requires temperatures in the vicinity of 550 °C.

Once formed, the parent layered materials can be exfoliated, and liquid phase exfoliation (LPE) [53] is the more commonly employed routine. It involves the use of ultrasonication or high-shear mixing to effectively peel off layers, to produce single or a few stacked layers [53]. Another interesting exfoliation approach is based on the formation of intercalation compounds [54,55]. In this case, the intercalation compound is formed by the insertion of ions, atoms or molecules into the interlayer spacing of the bulk material. This, in turn, gives rise to an increase in the interlayer distance, weakening the van der Waals forces, making it easier to deliver the exfoliated sheets. Nevertheless, processing of the parent layered material to give 2D monolayers or a few layered sheets can vary greatly, depending on the materials. For example, the production of 2D MXenes normally involves etching of the Al layers, and this requires aggressive HF etching, or fluoride salts combined with HCl, to oxidize the Al and form Al^{3+} in solution [37]. As illustrated in Equations (4)–(6), etching of the Ti_3AlC_2 MAX phase gives MXenes with –F and –OH terminal groups, $Ti_2C_3F_2$ or $Ti_2C_3(OH)_2$. The surface terminal groups depend on the composition of the etching solution, with the addition of HCl giving rise to –Cl terminal groups.

$$Ti_3AlC_2 + 3HF \rightleftharpoons AlF_3 + Ti_3C_2 + \frac{3}{2}H_2(g) \tag{4}$$

$$Ti_3C_2 + 2H_2O \rightleftharpoons Ti_3C_2(OH)_2 + H_2(g) \tag{5}$$

$$Ti_3C_2 + 2HF \rightleftharpoons Ti_3C_2F_2 + H_2(g) \tag{6}$$

On the other hand, the liquid phase exfoliation of bulk MoS_2, g-C_3N_4, h-BN and LDHs can be achieved more readily, to produce a few atomic layers of nanoplatelets [56,57]. However, the electrostatic interactions and the interlayer hydrogen bonding between the LDH layers can make the exfoliation process in water-containing solvents complex, and it can be difficult to avoid the restacking of the layers. While LPE is used extensively in the formation of single and a few layered nanosheets, the yield, quality, size and size dispersion of the 2D sheets depend on the solvent, sonication time and energy, and can be difficult to control. The influence of the solvent system is evident in Figure 3, wh ere it is clear that poly(2-butyl aniline) (PBA) can considerably enhance the dispersion of h-BN and its stability. On the other hand, the h-BN agglomerates following a 24 h storage period in the absence of PBA.
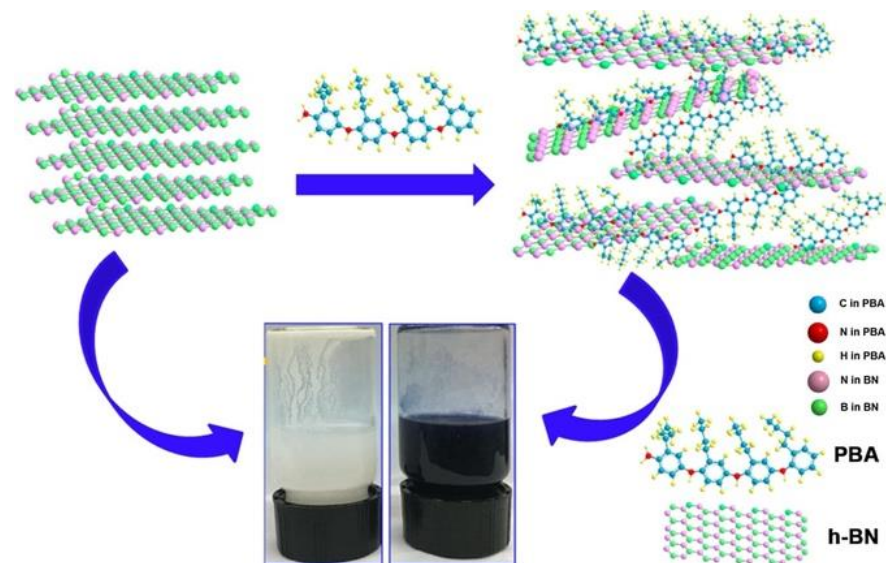

Figure 3. Illustration showing the influence of PBA on the dispersion of h-BN in THF (left: h-BN in THF, right: h-BN in THF and PBA). Reprinted with permission from Cui et al. [58], copyright Elsevier, 2018.

3. Coatings and Corrosion Protection

Corrosion-protective coatings have become the focus of considerable attention in a wide variety of applications [59], as they provide a barrier between the environment and the substrate metal or alloy. A number of very good reviews are available, describing the variety of coatings that have been employed, their roles in protecting metals and alloys in different environments and the events that lead to their loss of protection [60,61]. The ideal coating should provide an impermeable barrier to moisture and corrosive species, and exhibit long-term stability without cracking or delamination, which are the main failure mechanisms. In this regard, layered and 2D materials are interesting, as they can enhance barrier protection by impeding the diffusion of oxygen, water and corrosion-promoting ions, such as chloride anions. In theory, the impermeable nature of the 2D sheets can not only impede diffusion, but they can also be exploited to fill pores in the coatings, extending their protection period. In addition, smart coatings that can exhibit self-healing characteristics at defective sites, which would otherwise develop into corrosion sites, are especially interesting, and LDHs [62,63] and MXenes [64] can potentially serve as corrosion inhibitor nanocarriers.

In assessing and measuring the corrosion-protective efficiency of coatings, a number of experimental techniques and parameters can be employed, and these include corrosion current density (j_{corr}) and corrosion potential (E_{corr}) measurements, electrochemical impedance spectroscopy, salt spray tests, humid air environments and scratch tests. The j_{corr} and E_{corr} parameters provide useful information in the analysis of coatings, with j_{corr} being a measure of the rate of the corrosion reaction and E_{corr} representing a thermody-

namic factor. The Butler–Volmer equation (Equation (7)), can be applied to the corrosion reaction, which comprises both the anodic and cathodic electron transfer half reactions. In this analysis, $E - E_{corr}$ corresponds to the overpotential, and α_a and α_c are the charge transfer coefficients for the anodic and cathodic reactions, respectively.

$$j = j_{corr}\left(e^{\alpha_a F(E-E_{corr})/RT} - e^{-\alpha_c F(E-E_{corr})/RT}\right) \tag{7}$$

A protective coating should ideally have a much lower j_{corr} value than the corresponding uncoated substrate. Depending on whether the coating impedes the reduction reaction or the oxidation half reaction, the E_{corr} value can shift in a negative or positive direction. When the anodic oxidation reaction is inhibited, a lower j_{corr} is observed, while E_{corr} adopts a more positive value. Similarly, if the rate of the reduction reaction is lowered, then E_{corr} is shifted to more negative values and j_{corr} decreases. This can be explained using mixed potential theory [21]. These parameters are normally obtained from slow scan polarization curves [65], while cyclic polarization curves can also be very useful in determining the re-passivation characteristics [66].

However, these analyses are not suitable for organic coatings with high ohmic resistances, as the potential drop across the polymer layer is much larger than that across the metal-polymer interface. Accordingly, electrochemical impedance spectroscopy is frequently employed in the analysis of high-resistance organic coatings [67]. This technique is especially useful as it can be employed to monitor water uptake, which normally alters the capacitance of the organic coating, while events such as corrosion at the polymer/metal interface and the formation of defects in the coating alter the impedance [67]. Impedance measurements are also employed in a wide range of coatings with lower resistances, such as LDHs [68]. The impedance data can be fitted to equivalent circuits, or the coating performance can be assessed by monitoring the impedance at low frequencies in the vicinity of 10 mHz [69].

Accelerated corrosion tests in humid air, humid air with gaseous contaminants and salt spray tests are commonly used to evaluate the performance of coatings [70]. The salt spray tests are typically carried out in a NaCl spray at slightly elevated temperatures. The integrity of the coating and the build-up of corrosion products are monitored as a function of time. Scratch tests are very useful when it comes to smart corrosion-inhibitor-releasing coatings [71]. A scratch is made in the protective coating, and the coating's self-healing capacity can be assessed by monitoring the extent of corrosion at the created defect. The American Society for Testing Materials (ASTM) has developed a number of standard methods (for example, ASTM B117, which is a salt spray test) to evaluate localized and general corrosion, and these are very useful in assessing and comparing the corrosion-protective properties of new coatings.

While 2D materials are frequently used as fillers in organic and waterborne coatings [72], they have also been applied directly to the substrates [73]. Additionally, 2D materials with semiconducting properties can be employed in photocathodic protection [74,75]. These emerging layered materials have potential applications in the protection of metals and alloys in marine environments [76], in the protection of steel in concrete [77], as fillers in coatings for applications in transport and infrastructure (such as buildings and pipelines) and they can also serve to protect substrates at high temperatures [78]. In the following sections, each of the layered and 2D materials and their applications in the formulation of protective and anticorrosion coatings are described and reviewed.

3.1. Layered Double Hydroxides

Although LDHs can be exfoliated, it is normally the layered LDHs and not the 2D LDH nanosheets/nanoplatelets that are employed in the design of the current corrosion-protective coatings. Two main approaches have emerged: the LDHs can be synthesized and then applied to the corrosion-susceptible metal or alloy using for example spin coating [79], or an in situ approach is possible, especially with Al- and Mg-based systems [80]. It

is generally accepted that this in situ method, where the substrate provides the cations required for nucleation of the LDHs, is more promising due to the good adhesion between the substrate and the LDH.

As detailed in Table 1, LDHs can be conveniently fabricated using hydrothermal synthesis, where H$_2$O is employed as the solvent system. Typically, the LDH precursors are combined in solution and then autoclaved at relatively low temperatures, in the vicinity of 80° to 150 °C [81,82]. This methodology can be easily tailored to deposit the LDHs directly onto a metal or alloy substrate. For example, Hou et al. [80] formed a Mg-Al-LDH by placing the Mg substrate in an alkaline Al(NO$_3$)$_3$ solution, which was then transferred to an autoclave reactor and heated at 120 °C for 12 h. This is an effective way of depositing adherent LDHs onto corrosion-susceptible substrates. It relies on the oxidation of the substrate during the hydrothermal process to produce the divalent or trivalent cations required to form the LDHs. It has been used to deposit LDHs directly onto Al and Mg and their alloys [80–83], as Al^{3+} and Mg^{2+} cations are generated in situ during the hydrothermal reaction. An adaption of this method was used by Zhang et al. [73] to fabricate a Mg-Fe-LDH on a Mg substrate. Initially, an amorphous FeOOH film was electrochemically deposited on the Mg substrate, and then the LDH was nucleated by hydrothermal treatment in pure water to produce the Mg-Fe-LDH. Alternatively, divalent and trivalent precursors can be combined in the solution phase, and employed to nucleate the LDH onto the substrate. This methodology was employed to nucleate Zn-Al-LDH onto a Mg alloy. In this case, Zn(NO$_3$)$_2$ and Al(NO$_3$)$_3$ salts, at a concentration ratio of 2:1, were combined with the Mg alloy and heated in an autoclave at 80 °C for 12 h.

Due to the elevated temperatures employed in hydrothermal synthesis, LDHs with good crystallinity can be formed. In addition, other components, such as graphene oxide (GO) [84,85] and corrosion inhibitors [86], can be easily combined with the LDHs in a one-step hydrothermal experiment, as illustrated in Figure 4. Using this approach, Yan et al. [84] formed graphene-modified LDHs by dispersing GO with the Zn(NO$_3$)$_2$ and Al(NO$_3$)$_3$ precursor salt solution, while corrosion inhibitors, namely aspartate and laurate anions [86], were incorporated into the LDH in a single step. Clearly, hydrothermal synthesis exhibits high flexibility in terms of additives, morphology, crystal orientation, and structure of the final LDH. Nevertheless, the hydrothermal method requires temperatures elevated above room temperature and reaction times of several hours. Accordingly, the co-precipitation method is more widely employed.
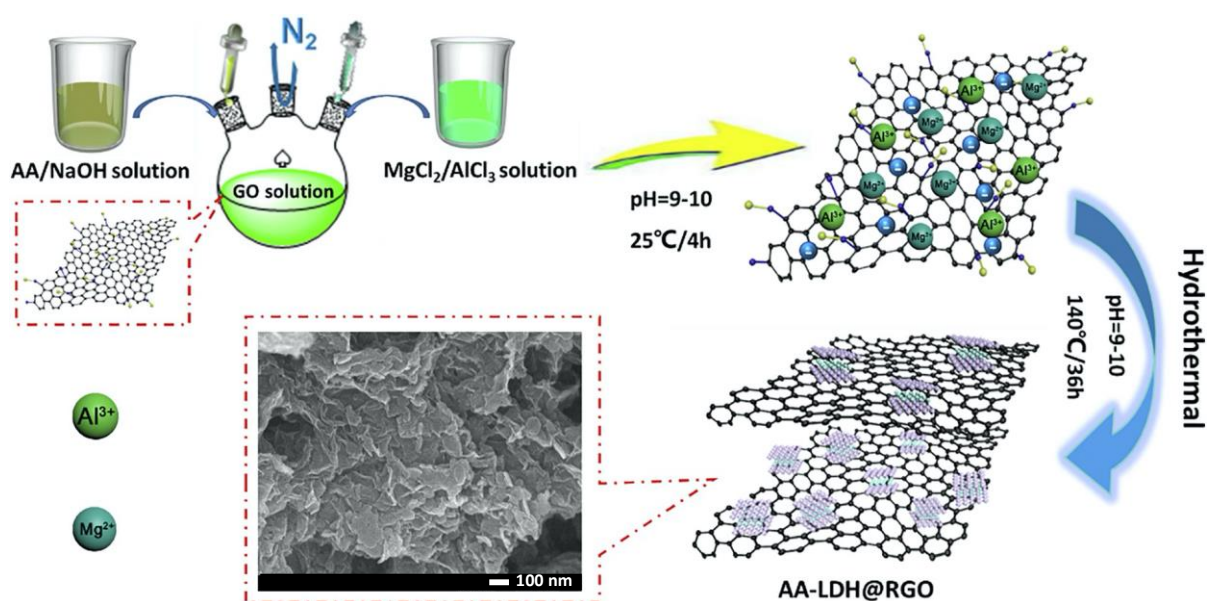

Figure 4. Schematic representation of the preparation of aspartic acid intercalated LDH/rGO hybrids. Reproduced with permission from Zhong et al. [85], copyright Elsevier, 2019.

In co-precipitation, a wide range of interlayer anions, including various corrosion inhibitors, can be employed, and the synthesis is suitable for upscaling. Typically, hydrated chloride or nitrate salts are used, but also it is possible to form LDHs using oxide phases, such as MgO [77]. It has been shown that the crystallinity of the LDHs can be improved by using the hydrolysis of urea [79,87]. This slow and progressive hydrolysis reaction maintains an alkaline environment through the generation of carbonates, which then become the interlayer anions. Ferreira et al. [31] used the co-precipitation method to synthesize Zn-Al-LDH, to produce the precipitation of vanadate-loaded LDHs. These LDHs were subsequently dried and processed as powders, added to a commercial paint and used to protect AA2024. In this routine, $Zn(NO_3)_2$ and $Al(NO_3)_3$ were dissolved and combined with $NaVO_3$. The pH of the slurry was maintained constant at 9.5 by the addition of NaOH over a 90 min period at 25 °C. Co-precipitation is also widely employed to produce the in situ deposition of LDHs, as this tends to provide good adhesion between the LDHs and the corrosion-susceptible substrates [88].

Although LDHs are more frequently deposited onto Al- and Mg-based substrates, they have been employed in the corrosion protection of copper and its alloys [89–91] and iron and steels [92–94]. In a recent report, Nikhil and Prakash [89] used the co-precipitation method to initially form the LDH, which was then placed with the copper substrate in an autoclave and subjected to the hydrothermal approach. This resulted in the deposition of the LDH onto the copper substrate. Similarly, Zuo et al. [94] formed a Mg-Fe-LDH protective film on a steel plate using the hydrothermal method. The steel was placed in the autoclave with a magnesium salt and urea to produce the in situ formation of the LDH on the steel substrate.

It is well known that the experimental conditions employed in both hydrothermal and co-precipitation synthesis can influence the properties of the fabricated LDHs [87]. Experimental parameters such as the concentration of reactants, pH, temperature and aging can all influence the particle size, morphology and crystallinity of LDHs, as illustrated in Figure 5, where the influence of pH is summarized. In general, the crystallinity is enhanced with increasing temperatures. In a recent study, LDH thin films were formed on AA6082 using the hydrothermal method, and the influence of temperature (from 40 to 100 °C) and treatment time (from 12 to 24 h) were studied [82]. It was found that the LDH coating formed at 100 °C for 18 h adopted a more dense and compact structure, and exhibited the highest corrosion-protective properties. In a related study, the same group found that the more corrosion-protective LDH coating was formed on AA6082 at a pH of 6.5 combined with a reaction time of 18 h at 80 °C [95]. Likewise, Alibakhshi et al. [96] have shown that the interlayer spacing depends on the pH employed during co-precipitation. At high pH values in the vicinity of 11.5 to 12.5, a decrease in the interlayer spacing was observed, while at lower pH values of about 9.5 a higher amount of nitrate and a low carbonate content gave rise to a closer spacing between the layers. Interestingly, the higher interlayer spacings resulted in better corrosion inhibition, and this was attributed to a higher nitrate concentration (which acts as an inhibitor) and greater chloride entrapment. It is also very well known that carbonates are very difficult to remove from LDHs, and a nitrogen atmosphere to exclude CO_2 is required to prevent the incorporation of carbonate within LDHs [93]. These studies demonstrate the importance of experimental parameters in the formation of LDHs.
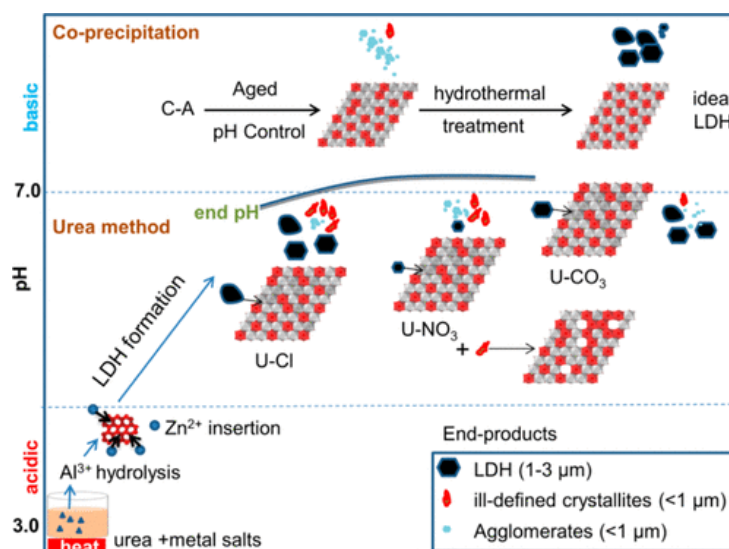
Figure 5. Influence of pH and synthetic methods on the structure of Zn-Al-LDHs. Reprinted with permission from Pushparaj et al. [87], copyright American Chemical Society, 2015.

The corrosion-protective properties of LDHs are normally attributed to a barrier effect, coupled with their anion exchange capacity. These anion exchange characteristics can be exploited to provide the controlled release of corrosion inhibitors. By loading LDHs with appropriate corrosion inhibitors, a triggered protection mechanism can be initiated, whereby the inhibitors are released in response to some change, such as pH, at a developing corrosion site. As a result, the corrosion event is halted [97–99]. This has the potential to give long-term corrosion protection. Various corrosion inhibitors have been incorporated as the anionic species within LDHs, and these include inorganic compounds such as molybdate [100–103], permanganate [104], nitrate [105–107], nitrite [77,108,109], phosphate [62], phenylphosphonate [110] and vanadate [111–113]. Also, organic inhibitors such as benzoate, 3-aminopropyltriethoxysilane, 8-hydroxyquinoline [63], 5-aminoindazole [90], benzotriazole [114], mercaptobenzothiazole [96,115,116], 2-mercaptobenzothiazole [117], thiophene derivatives [118], aspartic acid [119], 8-hydroxyquinoline [120], triazoles [121], α-amino acids [122] and 2-benzothiazolylthio-succinate [123] have been incorporated as the anionic species in LDHs. These inhibitors can be incorporated in a single step during the synthesis of LDHs, or by a two-step process, where the LDH is formed and then through anion exchange the anionic inhibitors are introduced [31,98]. However, with the narrow spaces that exist between the interlayer galleries, it can be difficult to insert the larger organic inhibitors as anions. Ma et al. [90] used an interesting approach to incorporate the organic inhibitor 5-aminoindazole into the interlayer spacings of Mg-Al-LDHs. The authors initially formed the nitrate-intercalated Mg-Al-LDH. Next, the LDH was exfoliated to give single-layered nanosheets, enabling the stripping of the nitrates. Finally, the nanosheets were reassembled with the organic inhibitor. In addition, the anion exchange process depends on the nature of the anions. It is very difficult to exchange carbonate anions, and to a lesser extent, nitrate anions. The exchange of these anions normally involves a two-step process, with deintercalation of the carbonate or nitrate, followed by intercalation of the desired anion. For example, LDHs intercalated with CO_3^{2-} can be transformed through calcination at about 500 to 550 °C to an oxide phase, as seen in Equation (8). The resulting oxide phase can then be rehydrated to restore, or partially restore, the original layered structure, while incorporating the desired anions [124]. However, this methodology is time-consuming and the LDH is not always fully restored.

$$Mg_{1-x}Al_x(OH)_2(CO_3)_{x/2} \rightarrow Mg_{1-x}Al_xO_{1+x/2} + x/2CO_2 + H_2O \qquad (8)$$
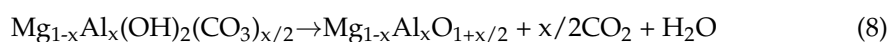
As the anionic corrosion inhibitors are released from the LDH network, they are replaced by incoming anions, which are normally chloride anions [125]. This in turn gives rise to the entrapment of the aggressive chloride anions, as illustrated in Figure 6. This is a somewhat surprising but interesting concept. There is clear evidence that the release of the inhibitors provides good corrosion-protective properties, while the aggressive and unwanted chloride anions are trapped, and this can be beneficial in terms of mopping up aggressive chloride anions. However, if these chloride anions are subsequently exchanged with other anions, it may give rise to elevated chloride concentrations.
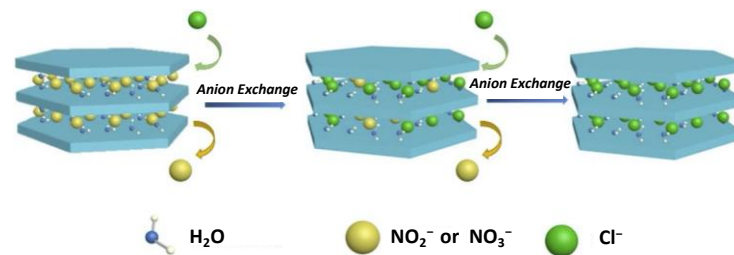

H_2O NO_2^- or NO_3^- Cl^-

Figure 6. Schematic representation of the anion exchange process and trapping of corrosion-aggressive anion chlorides. Adapted with permission from Zou et al. [77], copyright Elsevier, 2019.

In addition, LDHs can be combined with oxidized Al substrates, where the Al substrate is first oxidized through a plasma electrolytic oxidation (PEO) process [126,127]. This is a rapidly growing research area, as LDHs can seal the pores in the PEO [127,128], and this leads to an improvement in corrosion protection. Furthermore, corrosion inhibitors can be introduced as the anions in the LDHs, exploiting their inhibitor release and self-healing properties. For example, Ferreira et al. [96] employed Zn-Al-LDHs loaded with vanadate anions to seal the pores in the PEO with intercalation of the vanadate anions into the pores. This sealing suppressed the corrosion process. In a related study, the same group devised a method to facilitate the growth of LDHs on thick PEO coatings on aluminum-based substrates [128]. This was achieved by using sol-gel chemistry to create an aluminum oxide-based xerogel on the PEO, which provided a source of aluminum ions to facilitate the nucleation of the LDHs. Likewise, PEO coatings have been formed on Mg alloys, or the alloys have been anodized to create the oxide phases and combined with LDHs to produce an improvement in the corrosion protection properties of Mg alloys [129–133]. Furthermore, LDHs have been employed to provide corrosion inhibition on PEO-coated Mg-LDH [134,135].

Although LDHs have been shown to be effective in corrosion protection, and the PEO-oxidized substrates enhance corrosion protection, the LDH network is porous, with intercalated water molecules. This in turn provides a pathway for the diffusion of oxygen, which can be reduced at cathodic sites. As this reduction reaction proceeds, the dissolution of the metal is promoted, leading to local acidification. As a result, degradation of the LDH film can occur. Various attempts have been made to suppress the diffusion pathway by adding additional components. One of the more successful additives is graphene, which has a sealing effect due to its impermeable nature [136–138]. In addition, the negative charge on graphene oxide (GO), combined with the positively charged LDHs, facilitates the in situ growth of LDHs on the GO sheets, creating a network that greatly reduces permeability and consequently enhances corrosion resistance [84]. In addition, nanoparticles such as WO_3 [139], zirconia [140] and Al_2O_3 [141] can also serve to inhibit diffusion within the LDH network.

In Table 2, some of the more recent LDH composites and their corrosion-protective properties are summarized. While pristine LDHs can provide corrosion-protective properties, their performance can be enhanced considerably by the addition of corrosion inhibitors and additives that can alter the diffusion pathway. As illustrated in Table 1, some of the lowest corrosion currents and/or highest resistance values are seen with added corrosion inhibitors [142], graphene [143] and metal organic frameworks (MOFs) [144].

Table 2. Summary of some recent LDH composites and their corrosion protection properties.

LDH	Additive	Method	Measure of Corrosion Protection	Ref.
Mg-Fe	-	hydrothermal	$R = 2.0 \times 10^3 \ \Omega \ cm^2$ Q235 steel	[94]
Ca-Al	Mn	co-precipitation	$R = 5.2 \times 10^5 \ \Omega \ cm^2$ 2024-T3	[104]
Mg-Al	Ni layer	hydrothermal	$R = 6.48 \times 10^3 \ \Omega \ cm^2$ AZ31B Mg	[145]
Mg-Al	benzoate/perfluoro-decyltrimethoxysilane	hydrothermal	$\|Z\|/0.01 Hz = 1.76 \times 10^6 \ \Omega \ cm^2$ AZ31 Mg	[69]
Mg-Al	5-aminoindazole	co-precipitation/ hydrothermal	$R = 31 \times 10^3 \ \Omega \ cm^2$ $j_{corr} = 3.2 \times 10^{-7}$ A cm^{-2}/Cu	[90]
Mg-Al	Ce/NO$_3^-$	co-precipitation	$j_{corr} = 2.2 \times 10^{-7}$ A cm^{-2} AZ31 Mg alloy	[146]
Mg-Al	sodium dodecyl sulfate	co-precipitation/ hydrothermal	$j_{corr} = 2.2 \times 10^{-8}$ A cm^{-2} $R = 4.38 \times 10^7 \ \Omega \ cm^2$ AZ31 Mg alloy	[142]
Mg-Al	8-hydroxyquinoline/GO	hydrothermal	$j_{corr} = 1.44 \times 10^{-9}$ A cm^{-2} AZ31 Mg alloy	[143]
Mg-Al	poly(ethyleneimine)/MXene, V$_2$O$_7^{2-}$	hydrothermal	$j_{corr} = 1.3 \times 10^{-8}$ A cm^{-2} $R = 3.2 \times 10^6 \ \Omega \ cm^2$ AZ31 Mg alloy	[147]
Mg-Al	albumin-WO$_3$	co-precipitation	$R = 4.46 \times 10^9 \ \Omega \ cm^2$ AZ31 Mg	[139]
Mg-Al	8-hydroxyquinoline/sol-gel	co-precipitation/ hydrothermal	$R = 9.1 \times 10^6 \ \Omega \ cm^2$ AM60B alloy	[68]
Zn-Al	benzotriazole/(MOF)/ polyvinyl butyral	co-precipitation/ hydrothermal	$j_{corr} = 2.0 \times 10^{-12}$ A cm^{-2} Cu	[144]

3.2. Transition Metal Dichalcogenides

In recent times, there has been considerable interest in TMDs, such as MoS$_2$, WS$_2$, MoSe$_2$ and WSe$_2$, because they possess properties similar to graphene in terms of their 2D sheet-like structures. MoS$_2$ has been employed in the protection of semiconductors, such as GaInP$_2$ (gallium indium phosphide), which are susceptible to chemical and electrochemical corrosion in aqueous electrolytes [148] and silicon-based photocathodes [149]. However, research into its applications in the corrosion protection of metals and alloys is still in its infancy. It has been shown in several studies that MoS$_2$ has excellent mechanical properties [150], making it an interesting candidate in the formulation of corrosion-protective coatings. Indeed, there is evidence from the literature to show that the addition of MoS$_2$ can improve the protective properties of coatings on metals or alloys [151–153].

In a recent study, Ding et al. [151] prepared MoS$_2$ nanosheets by exfoliating bulk MoS$_2$, followed by the collection of the 2D nanosheets through centrifugation. Then the nanosheets were combined with an epoxy curing agent to give a TMD/EP nanocomposite, which was painted onto steel and cured at 50 °C. The wt% of MoS$_2$ in the epoxy coating was varied, and it was found that the best corrosion protection was achieved with a 1.0 wt% MoS$_2$/EP. Using oxygen transmission and water vapor transmission rates, the impermeability of the prepared nanocomposite coatings was evaluated. The authors found that the MoS$_2$/EP coatings possessed good barrier properties, impeding the transport of both oxygen and water. The authors explained the observed corrosion protection in terms of reduced permeability and the low conductivities of the semiconductor TMDs, thus inhibiting galvanic corrosion, which is seen when graphene is employed in coatings [22]. In addition, it was concluded that the few layered MoS$_2$ nanosheets were ineffective in

catalyzing the oxygen reduction reaction. Similarly, Zhao et al. [154] found that epoxy coatings containing MoS_2 dispersed with sodium dodecyl benzene sulfonate reduced the water-permeability of the coating. Interestingly, greater adhesion between the coating and substrate was seen in the presence of the MoS_2, giving rise to a reduction in the rate of coating delamination.

Hong et al. [153] dispersed MoS_2 in sunflower oil, and applied this dispersion onto a stainless steel (SS 316L) substrate, which was then subjected to heating to polymerize the triglycerides in sunflower oil. As a result, an adherent polymeric coating with MoS_2-dispersed sheets/particles was formed. Good corrosion protection and durability was seen with the MoS_2-containing sunflower coating, and this was attributed to the formation of a highly ordered barrier coating. Likewise, ArunKumar et al. [155] dispersed MoS_2 and doped MoS_2 in sunflower oil, and found that doping MoS_2 with Fe, Co, and Ni ions resulted in an increase in the corrosion-protective properties of MoS_2. For example, the corrosion current of mild steel was measured as 83×10^{-6} A cm^{-2} in a chloride-containing solution. On modifying the steel with MoS_2, the current was reduced to 5×10^{-9} A cm^{-2}, but it was reduced further to 3×10^{-9} A cm^{-2}, 2×10^{-9} A cm^{-2} and 1×10^{-9} A cm^{-2} for Co-, Ni- and Fe-doped MoS_2, respectively. This is interesting, as metal ion doping generally increases the electrocatalytic activity of MoS_2 [156]. While this approach may be promising at short times, these more conductive metal-doped MoS_2 sheets may behave like graphene at longer times and promote galvanic corrosion.

On comparing WS_2 with MoS_2 in the formulation of corrosion-protective coatings on a Mg–Li alloy, Li et al. [157] found that a more compact and hydrophobic coating was formed with WS_2, to give significantly enhanced corrosion protection over an extended immersion time. Likewise, Prado and Virtanen [152] exploited the hydrophobic characteristics of MoS_2 to form a superhydrophobic metal matrix composite coating by adding MoS_2 particles to a copper matrix. This was then applied to two steel substrates, SS 316L and CS N80. It has also been shown that the addition of MoS_2 has beneficial effects in the performance of polyvinyl butyral and zinc-rich polyvinyl butyral coatings [158]. Furthermore, on incorporating MoS_2 into conducting polymers, such as polypyrrole and polyaniline, their protective properties can be enhanced [159,160]. In these cases, MoS_2 was incorporated during the electropolymerization step, and it has been suggested that the MoS_2 blocks voids within the porous polymers, reducing the transport of oxygen and water to the substrate [159].

Given the semiconducting properties of TMDs, they are attractive in photoelectro-chemical cathodic corrosion protection [74]. This is similar to cathodic protection, where a potential or current is applied to the metal surface to polarize it below its corrosion potential and into the immune region (Figure 7) [161]. In photocathodic protection, electrons are excited from the valence band into the conduction band of the n-type semiconductor, and these are then coupled with the corrosion-susceptible metal or alloy, resulting in polarization into the immune region. Compared to sacrificial anodes, which provide corrosion protection by preferentially dissolving and producing metal ions while protecting the desired metal, photocathodic protection is environmentally acceptable.

TMDs such as MoS_2 have small band gap energies, and therefore the electron and hole pair can be generated using visible light. For example, MoS_2 has been combined with TiO_2 to facilitate the absorption of visible light, and to suppress the recombination of electron-hole pairs in TiO_2. This is achieved by forming a p-n heterojunction with TiO_2 to give separation of the photogenerated carriers [74]. It has been shown that on absorption of visible light, the potential of the SS304 substrate coupled to the MoS_2/TiO_2 nanocomposite dropped by approximately 500 mV, giving cathodic protection. Furthermore, when the light source was removed and then turned on again, the same potential drop was observed, indicating very good stability of the MoS_2/TiO_2 nanocomposite.
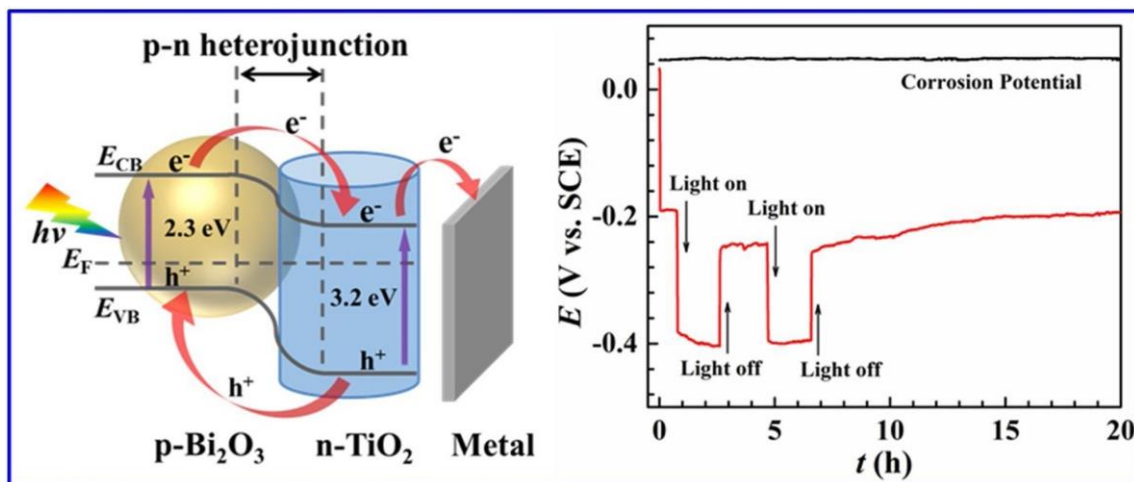
Figure 7. Schematic representation of a p-n heterojunction enabling the transfer of electrons to the metal surface, which shifts its potential in the negative direction, bringing the metal into its immune region. Reprinted with permission from Guan et al. [161], copyright Elsevier, 2018.

3.3. MXenes

MXene nanosheets have a rich surface chemistry, large specific surface areas, and very good mechanical properties with good thermal and electrical conductivity. They are attracting a lot of attention in corrosion research, especially as additives in polymer composites. MXenes have a unique multilayer structure, which is composed of numerous parallel sheets, as illustrated in Figure 2C. These sheets can act as a barrier to the diffusion of oxygen and aggressive ions, such as chlorides. Indeed, Yan et al. [72] observed a considerable reduction in the corrosion current from 7.51×10^{-5} A cm^{-2} for bare Q345 to 3.38×10^{-8} A cm^{-2} for 1.0 wt% Ti_3C_2/epoxy. The 1.0 wt% MXene coating also exhibited the highest charge transfer resistance, with a value of 5.48×10^8 Ω cm^2 after 2 h and 2.82×10^7 Ω cm^2 after 96 h.

It is also possible to encapsulate molecules and ions between the MXene layers, and this can be exploited to load corrosion inhibitors that can be subsequently released in response to a corrosion event. For example, Haddadi et al. [64] functionalized Ti_3C_2 with NH_2 groups and loaded the MXene with Ce^{3+}, a well-known corrosion inhibitor. The Ce^{3+}-containing MXene was dispersed in epoxy to provide a coating. The protective properties of the epoxy coating, EP, MXene-EP and MXene-EP-Ce^{3+} were compared. The corrosion current was reduced from 15.65×10^{-6} A cm^{-2} to 13.90×10^{-6} A cm^{-2} upon incorporation of the MXene, and reduced further to 3.16×10^{-6} A cm^{-2} with the addition of Ce^{3+}. Using a combination of Ce^{3+} release studies and impedance and salt spray tests, the authors clearly showed that MXene-EP-Ce^{3+} was the superior coating. This was attributed to the release of the Ce^{3+}, which acts as a cathodic inhibitor. This is illustrated in Figure 8.

Furthermore, MXenes can be functionalized using their terminal groups [162,163]. Recently, epoxy-functionalized Ti_3C_2 nanosheets were formed by grafting the MXene with (3-glycidyloxypropyl) trimethoxysilane [72]. This functionalized MXene was then incorporated into an epoxy coating. It was found that the functionalized MXene gave the highest corrosion protection, when compared to the non-functionalized MXene. This was explained in terms of higher dispersibility and chemical bonding within the matrix with the functionalized MXene. Other functionalized groups have been successfully employed, and these include L-cysteine [164], chitosan [165], and amino groups [166]. These are normally covalently attached to the surface of MXenes, and then incorporated within an epoxy to make well-dispersed nanosheets with good barrier protection properties. In addition to epoxy coatings, MXenes have also been combined with silane-based coatings to improve the quality of silane-based systems. The hydrophilic groups on the MXene give rise to good dispersion of the MXene in the silane coatings, and this avoids structural defects.

MXenes have been introduced into silane films using γ-glycidoxypropyltrimethoxysilane to deposit composite coatings on AA2024 aluminum alloy [167], and applied to copper using 3-mercaptopropyltriethoxysilane (mercaptosilane) [168]. The $Ti_3C_2T_x$/silane composite films have been shown to exhibit excellent adhesion and corrosion resistance, and can be prepared using a simple solution-based process.
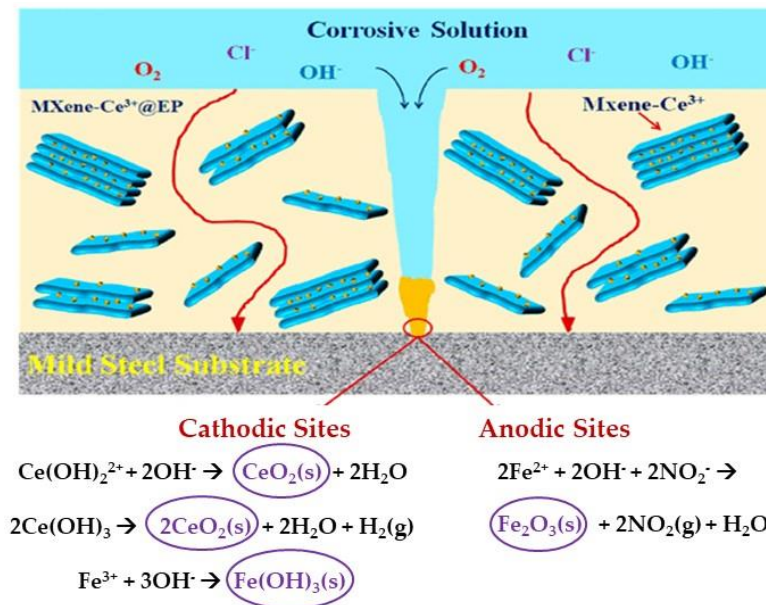

Figure 8. Schematic representation of the corrosion-inhibition mechanism of Ti_3C_2 MXene loaded with Ce^{3+} in the coating, with the released Ce^{3+} acting as a cathodic inhibitor. Adapted with permission from Haddadi et al. [64], copyright American Chemical Society, 2021.

Nevertheless, $Ti_3C_2T_x$ has high electrical conductivity, a hydrophilic surface, is prone to oxidation, has a natural restacking tendency and has relatively poor stability in water. These are characteristics that are not always desirable in the formulation of protective coatings. In particular, the high conductivity can promote corrosion, with the formation of a galvanic corrosion cell with the substrate. Indeed, there have been reports which clearly show that MXenes can facilitate corrosion [64]. By studying the interface interactions between $Ti_3C_2T_x$ and Fe, Cai et al. [64] showed that the corrosion of Q345, a mild steel, was accelerated by $Ti_3C_2T_x$. This was explained in terms of the high conductivity of MXene, which facilitated the oxygen reduction reaction, an important half-cell reaction in the corrosion cell.

Recently, there has been much focus on enhancing the stability of MXenes. $Ti_3C_2T_x$ MXene nanosheets are prone to oxidation in both air and water, and this oxidation reaction can give rise to the formation of oxides that can lead to further degradation of the MXene layered structure. This reduces the barrier protection afforded by the MXene sheets when used in protective coatings. Attempts have been made to enhance the corrosion protection properties of MXenes, and one methodology involves the formation of MXene hybrids or heterostructures. MXenes have been combined with several other materials, including carbon dots (CD) [169], graphene oxide (GO) [170], graphene [171], LDHs [172], h-BN [173], MoS_2 [174] and conducting polymers [175] to form composites or heterostructures. The addition of this second material can enhance the corrosion-protective performance of MXenes. For example, it is well known that MXenes are susceptible to hydrolysis reactions and have poor stability in water. The chemical stability of MXenes in water has been improved by using carbon dots (CD) to functionalize $Ti_3C_2T_x$ MXene and form a CD-$Ti_3C_2T_x$ hybrid [169]. Likewise, an OH-group-modified h-BN was utilized to reduce the formation of a conducting MXene network [173]. With the addition of LDHs, $Ti_3C_2T_x$ MXene/Mg-Al-LDH heterostructures can be formed [172], as shown in Figure 9. These

inhibit the restacking of the MXene to give very good dispersion throughout the coatings, with good compatibility with epoxy resin materials. Moreover, anionic corrosion inhibitors can be loaded onto LDHs. Restacking of MXenes can also be minimized by forming hierarchical $Ti_3C_2T_x/MoS_2$ heterostructures [174]. The interconnected MoS_2 nanosheets were anchored onto the MXene nanosheets, and as a result effectively prevented restacking of both the MXene and the MoS_2 nanosheets. On using this heterostructure as a filler in an epoxy coating, good anti-corrosion and anti-wear properties were observed. Using intercalation polymerization, aniline was polymerized to give polyaniline layers between the Ti_3C_2 sheets [175]. This was shown to reduce the conductivity of the MXenes, which is necessary to achieve long-term corrosion protection. It has been shown that ionic liquids, such as imidazolium salts, can passivate the MXenes, while the imidazolium salts can also act as corrosion inhibitors. Zhao et al. [176] have used this approach to form air-stable MXene-reinforced coatings. Not only did the ionic liquid protect the MXene from oxidation, it also provided good dispersion, increasing the barrier property of the coating with an additional self-healing capacity, due to the inhibiting properties of the imidazolium-based ionic liquid.
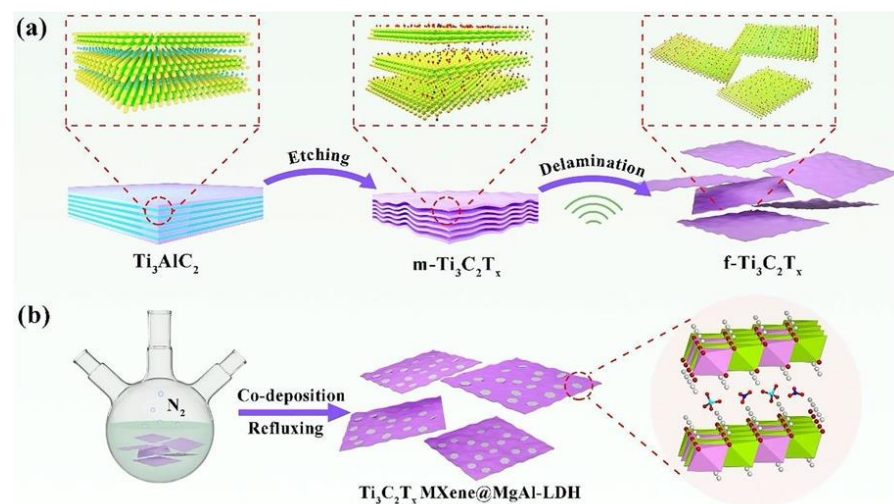

Figure 9. Schematic representation of the synthesis of (**a**) the $Ti_3C_2T_x$ MXene nanosheets and (**b**) formation of the $Ti_3C_2T_x$/Mg-Al-LDH heterostructure. Reprinted with permission from Cai et al. [172], copyright American Chemical Society, 2021.

3.4. Hexagonal Boron Nitride

Nanosheets of hexagonal boron nitride (h-BN) have similar characteristics as graphene, in terms of mechanical, thermal, hydrophobic and permeability properties. However, h-BN is an insulator, and this is one significant difference that makes h-BN more attractive than graphene as a component of coatings or protective films. With its insulating properties, it is very unlikely to promote galvanic corrosion. However, the lack of functional groups on the h-BN sheets make it difficult to functionalize the surface, compared to the ease at which GO can be functionalized. Furthermore, it can be difficult to disperse h-BN in aqueous solutions or waterborne epoxy matrices, owing to its hydrophobicity and strong interlayer van der Waals interactions.

Different approaches have been employed with the aim of forming stable dispersions of h-BN that can be employed in protective coatings. For example, it is possible to employ a non-covalent method whereby a suitable organic molecule is used to modify the h-BN nanoplatelets through π-π interactions. This has been achieved with amine-capped aniline trimers, resulting in a stable dispersion of h-BN nanoplatelets in organic solvents. This dispersion was subsequently used to form a 1.0 wt% h-BN/epoxy coating with good barrier properties, and good wear and corrosion resistance [177]. Similarly, a homogeneous dispersion of h-BN in an epoxy matrix was obtained using a water-soluble carboxylated aniline

trimer [178]. Again, this good dispersion was attributed to strong π-π interactions between h-BN and the trimer. Poly(2-butyl aniline) (PBA) [58] and furfuryl methacrylate [179] have also been employed to give well-dispersed h-BN in epoxy coatings, while ionic liquids, with their conjugated structures and nitrogen atoms, facilitate π-π interactions with the h-BN nanoplatelets [180]. In addition, GO, with hydrophilic characteristics, was employed as an intercalator to exfoliated h-BN and enhanced its dispersion. The π-π interactions between GO and h-BN gave rise to h-BN/GO stacks [181].

Alternatively, the h-BN can be chemically functionalized. Using this approach, Zhao et al. [182] employed a gas-assisted liquid exfoliation method to create hydroxyl-functionalized h-BN, which was subsequently phosphorylated. Wu et al. [183] and Yu et al. [184] treated h-BN with (3-aminopropyl) triethoxysilane (APTES) to functionalize its surface with an alkoxysilane, in order to create a homogenous dispersion of the functionalized h-BN in epoxy coatings. In addition, a Lewis acid–base reaction was performed to functionalize h-BN with water-soluble branched poly (ethyleneimine) [185], while h-BN was functionalized with polyacrylic acid through a plasma polymerization reaction [186]. It has also been shown that h-BN can be modified with epoxy groups and polydopamine, which is readily formed through the self-oxidation of dopamine in an alkaline solution. This relatively simple method was reported to provide good compatibility between the h-BN and the epoxy matrix, resulting in impressive corrosion-protective performance. These non-covalent and covalent modifications of h-BN enhance its dispersion in epoxy [58,178,180,181,183,185,187] and acrylic [186] coatings, giving rise to good corrosion-protective properties. The enhanced anticorrosive performance has normally been attributed to the homogeneously dispersed h-BN nanoplatelets, which provide very good water- and oxygen-barrier properties.

Other polymeric formulations have been employed with h-BN, and these include polyvinyl alcohol [76], polyimide [188], polyvinyl butyral [189] and waterborne polyurethane [190]. Using spin coating, Husain et al. [76] coated SS 316L with h-BN dispersed in polyvinyl alcohol (PVA). The PVA was used as a binder to increase the adhesion between the h-BN nanoplatelets and the steel surface. It was concluded that the h-BN films were effective at inhibiting corrosion. However, crevice and pitting corrosion were observed between the metal and coating interface. Interestingly, when h-BN was dispersed in waterborne polyurethane [190], the coating was shown to provide long-term corrosion protection for the underlying copper.

Protective h-BN deposits have also been deposited directly onto the substrate by using electrophoretic deposition [182]. In this case, dispersed h-BN and dispersed phosphorylated h-BN were electrophoretically deposited onto Q235 carbon steel substrates at applied potentials between 0.6 and 1.2 V. The corrosion current for the unmodified substrate was 17.74×10^{-6} A cm^{-2}, but lower values of 2.88×10^{-6} and 0.55×10^{-6} A cm^{-2} were observed for the electrophoretically-deposited h-BN and phosphorylated h-BN, respectively. However, with increasing immersion time, delamination of the deposits was observed. Magnetron sputtering has also been employed to deposit h-BN directly onto stainless steel (SS304) substrates [191]. These deposits showed good corrosion resistance over a 10-week period when immersed in a 3.5 wt% NaCl solution. Huang et al. [192] formed atomically thin h-BN films at 1000 °C and 1100 °C on solid and melted copper. The authors found that the quality of the h-BN atomic thin films was important, with water dissociation reactions evident at h-BN boundaries, leading to oxidation of the copper substrate. On the other hand, less-defective, high-quality films grown on melted copper showed impressive corrosion protection in 0.5 M NaCl.

Iron oxide nanoparticles (Fe_3O_4) have been combined and supported on h-BN to create corrosion-protective coatings [193]. Zhang et al. [193] employed hydrothermal synthesis to form Fe_3O_4 nanoparticles on the surface of h-BN. The h-BN-Fe_3O_4 hybrids were incorporated as fillers into epoxy resin to create protective coatings. The good corrosion protection was explained in terms of blocking of the micro-pores within the coating. The Fe_3O_4 nanoparticles supported on the h-BN nanoplatelets were less prone to

agglomeration, providing a more homogenous dispersed phase that reduced the transport of oxygen, water and aggressive chloride ions through the epoxy coating.

As h-BN and graphene share similar properties, direct comparisons of their anti-corrosion performance have been made [184,194–196]. Yu et al. [184] functionalized graphene, graphene oxide and h-BN with 3-aminopropyltriethoxysilane to form a series of waterborne epoxy composite coatings on Q235. Using a combination of Tafel analyses, electrochemical impedance spectroscopy measurements and immersion in a 3.5 wt% NaCl aqueous solution for different time intervals, the authors concluded that the composite coating with the functionalized h-BN exhibited the best performance. Scardamaglia et al. [194] studied the high-temperature oxidation of copper foils with thin layers of h-BN and graphene. It was found that both graphene and h-BN protected the Cu from oxidation. However, significant variations were seen on comparing both layers, with different reaction pathways. With h-BN, the copper was very well protected from oxygen, with the insulating nature of h-BN protecting the copper from oxidation, until a temperature of about 300 °C was reached, and the layers were etched. On the other hand, the intercalation of oxygen beneath the graphene flakes gave rise to the slow conversion of Cu to Cu_2O, while the galvanic reaction between the conducting graphene and Cu facilitated the oxidation process. Likewise, Galbiati et al. [197] concluded that the h-BN layer provides more effective protection of copper at elevated temperatures, with little evidence of oxidation after 60 hours at 50 °C, as shown by XPS and XAES measurements.

3.5. Graphitic Carbon Nitride

Graphitic carbon nitride (g-C_3N_4) is a polymeric semiconductor with high chemical and mechanical stability, and it is considerably more cost-effective than other carbon-based materials, such as carbon nanotubes. It is also hydrophobic in nature, and as a filler in a coating it can inhibit water drops from adsorbing onto the surface to restrict penetration of the corrosive species into the coating. Normally, g-C_3N_4 is employed as a filler in epoxy, and especially waterborne epoxy coatings [198], but it has also been combined with polystyrene [199], which is a more hydrophobic polymer, to protect copper from corrosion. Interestingly, Xu et al. [200] formed a self-healing coating capable of repairing its structure upon mechanical damage using poly(urea-urethane)/g-C_3N_4 nanosheets. This coating also exhibited good corrosion protection properties when applied to an aluminum alloy, protecting the aluminum substrate from corrosion in 0.5 M NaCl for a 20 day-period. It is normally the exfoliated 2D structures that are employed in the design of coatings, as they have the potential for more chemical interactions with other materials, enabling synergistic effects, and a much higher surface area compared to the bulk g-C_3N_4.

Nevertheless, agglomeration of the g-C_3N_4 nanosheets can easily occur, and this is a particular issue with water-based epoxy coatings [201]. As agglomeration occurs, the corrosion-protective efficiency of the nanocomposite coatings decreases significantly. The bulk g-C_3N_4 can be exfoliated in alcohols, such as isopropanol [202], but it is more challenging to maintain the 2D nanosheets dispersed in coating formulations or the final coatings. One approach that has been employed involves the use of a companion material [198,203]. For example, graphene oxide, which is hydrophilic as a result of its acidic functional groups, can facilitate the dispersion of g-C_3N_4 in waterborne epoxy polymers [198]. It was shown by XRD measurements that a GO/g-C_3N_4 hybrid was formed, with the g-C_3N_4 nanosheets attached on the GO nanosheets. Xia et al. [201] produced hydrophilic organic films to coat g-C_3N_4 nanosheets by modifying the g-C_3N_4 with polydopamine and a silane coupling agent. This not only enhanced the dispersion of g-C_3N_4, but improved its compatibility with the waterborne epoxy. Good corrosion protection was observed, as shown in the polarization plots depicted in Figure 10. Similarly, Sheng et al. [204] formed polydopamine-coated g-C_3N_4 and iron oxide as fillers for coatings. The dispersion ability of g-C_3N_4, α-Fe_2O_3, g-C_3N_4/α-Fe_2O_3 and polydopamine/g-C_3N_4/α-Fe_2O_3 were compared. The polydopamine-modified g-C_3N_4/α-Fe_2O_3 remained evenly dispersed for over 24 h. Very good corrosion protection was observed with the added polydopamine, and this was ex-

plained in terms of strong interfacial bonding between the polydopamine and epoxy matrix, combined with very good barrier protection from the nanofillers. Other materials used to enhance the dispersion of g-C$_3$N$_4$ in waterborne coatings or to enhance its mechanical properties as a filler include polyaniline formed on the surface of g-C$_3$N$_4$ [203], molybdenum oxides, MoO$_x$ [205], and SiO$_2$ with TiO$_2$ [206]. Also, g-C$_3$N$_4$ has been functionalized with ethylenediamine vapor to enhance its dispersion in a solvent-based epoxy [207]. Clearly, the 2D g-C$_3$N$_4$ nanosheets can be hybridized with other components to design more corrosion-protective coatings.
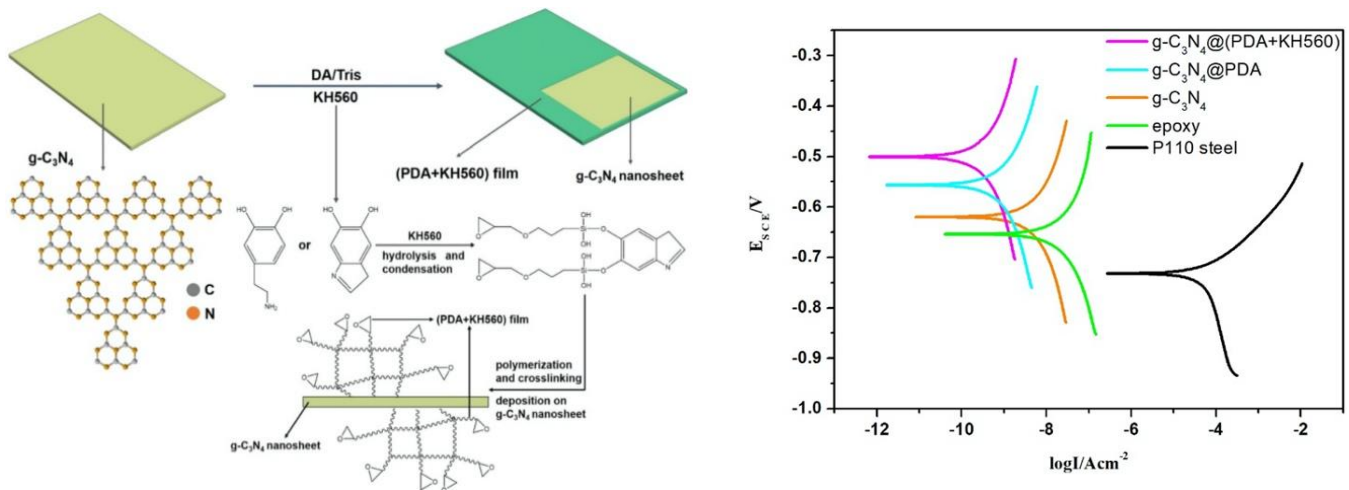

Figure 10. Schematic illustration of the preparation of the g-C$_3$N$_4$ nanocomposite (left) and polarization curves recorded after 15 days of immersion in an aqueous 3.5 wt% NaCl solution. Reprinted with permission from Xia et al. [201], copyright Elsevier, 2020.

As a photocatalyst, g-C$_3$N$_4$ is attracting considerable attention [208], and it has been studied and successfully employed in the photocathodic protection of SS316 and Q235 [209], Q235 CS [210] and SS 304 [75]. It has a relatively high charge carrier recombination rate, and therefore it is mostly combined with other semiconductors to create heterostructures. In a recent study, a g-C$_3$N$_4$/GO/MoS$_2$ composite was formed, and generated a photocurrent of 77.19 µA cm^{-2} when coupled with SS 304. In this case, the photogenerated electrons in the conduction band of g-C$_3$N$_4$ were transferred to the valence band of MoS$_2$, giving effective charge separation [75]. Other heterojunctions, including ZnO/g-C$_3$N$_4$ [211] and In$_2$O$_3$/g-C$_3$N$_4$ [212], have been utilized in photocathodic protection. Interestingly, Zhang et al. [209] formed g-C$_3$N$_4$ *n-n* homojunction films on indium tin oxide substrates. With the optimum photocathodic protection, photocurrents of 143.44 µA cm^{-2} and 111.48 µA cm^{-2} were observed for SS316 and Q235, and the potentials were lowered to -982 mV and -1081 mV, well into the immune region for SS316 and Q235.

4. Conclusions, Outlook and Future Directions

The corrosion of metals and alloys has always been an issue, but in recent years corrosion protection has emerged as a particular challenge, given the increasing focus on sustainability and environmental issues. Many of the corrosion-protective approaches used in the past have relied on chromates and volatile organics that are no longer environmentally acceptable. At the same time, metals and alloys have to function in new and extremely harsh environments, such as the blades of windmills, plates in fuel cells, or casings of batteries. While significant advancements have been made in structural materials, in terms of their mechanical properties, their ability to perform and withstand corrosion remains a particular challenge.

Fortunately, there has been an explosion in the development of new materials, spanning various nanostructured materials and 2D materials, and these are likely to contribute

to developments in corrosion protection in the near future. It is clear that the layered and 2D materials reviewed here are emerging as promising materials, and may provide new, environmentally-acceptable coatings that can protect metals and alloys. These 2D materials have been successfully employed in the formulation of anticorrosion coatings, frequently acting as coating fillers and impermeable sheets that increase barrier protection and reduce diffusion of oxygen, water and aggressive ions throughout the coating. They have been studied in different aggressive environments and at elevated temperatures, and have performed well. While 2D graphene has been studied extensively, there is now a consensus that the conducting properties of graphene promote galvanic corrosion with the substrate, and can in fact increase the corrosion rate. Therefore, 2D materials that have much lower conductivity than graphene, including h-BN, g-C_3N_4, and LDHs, are interesting, as they are unable to generate galvanic cells with the substrate, and may play a leading role in the development of new anticorrosion coatings. Relatively few studies have centered on evaluating TMDs in corrosion protection, and clear evidence to suggest that TMDs can provide corrosion protection is still lacking. Nevertheless, they have been employed to create superhydrophobic coatings, which is very relevant in the development of anticorrosion coatings. In terms of photocathodic corrosion protection, TMDs and g-C_3N_4, which exhibit semiconducting characteristics, are interesting. The band gap energies of both TMDs and g-C_3N_4 are small, and the necessary charge carriers can be generated using visible light.

Nevertheless, the true applications of these materials in corrosion protection are only emerging, and require further study before they can be applied extensively in the formulation of anticorrosion coatings. One avenue that requires further study, and is relevant to all 2D materials, is the exfoliation of the 2D sheets to give stable, well-dispersed sheets in organic and especially in waterborne coatings, which are more environmentally acceptable. When homogeneously dispersed, the 2D sheets can impede diffusion, however if the sheets become agglomerated their effectiveness is reduced considerably. Furthermore, the exfoliation efficiency of 2D materials can be low and require organic solvents, which limits the dispersion of 2D materials in waterborne coatings. On the other hand, LDHs are employed as layered materials. With this layered structure, corrosion inhibitors can be incorporated into the layered structure and released at corroding sites. However, this approach can lead to the incorporation and trapping of chloride anions. While this has the potential to mop up chloride anions, the longer-term impact of these trapped aggressive anions requires further study.

Another challenge is the synthetic processes required to generate both the parent and the 2D materials. The development of synthetic processes that can be easily upscaled and are cost-effective are essential. Therefore, high temperatures or high pressures that are typically employed with h-BN and the parent MAX phase of MXenes make these materials less cost-effective. The lower temperature methodologies, such as co-precipitation, although simple to carry out, have complex chemistry, making it more challenging to upscale the processes.

While challenges remain, it is clear that these 2D materials are likely to play a significant role in the development of protective and anticorrosion coatings into the future, as new synthetic methods for the functionalization of 2D materials are developed, facilitating their improved dispersion in coating formulations.

Data Availability Statement: Not applicable.

Conflicts of Interest: The authors declare no conflict of interest.

References

1. Heinz, A.; Haszler, A.; Keidel, C.; Moldenhauer, S.; Benedictus, R.; Miller, W.S. Recent development in aluminium alloys for aerospace applications. *Mater. Sci. Eng. A* **2000**, *280*, 102–107. [CrossRef]
2. Miura, S.; Honma, H. Advanced copper electroplating for application of electronics. *Surf. Coat. Technol.* **2003**, *169–170*, 91–95. [CrossRef]
3. Baddoo, N.R. Stainless steel in construction: A review of research, applications, challenges and opportunities. *J. Constr. Steel Res.* **2008**, *64*, 1199–1206. [CrossRef]
4. Ryan, M.P.; Williams, D.E.; Chater, R.J.; Hutton, B.M.; McPhail, D.S. Why stainless steel corrodes. *Nature* **2002**, *415*, 770–774. [CrossRef] [PubMed]
5. Yellishetty, M.; Ranjith, P.G.; Tharumarajah, A. Iron ore and steel production trends and material flows in the world: Is this really sustainable? *Resour. Conserv. Recycl.* **2010**, *54*, 1084–1094. [CrossRef]
6. Frankel, G.S. Pitting corrosion of metals: A review of the critical factors. *J. Electrochem. Soc.* **1998**, *145*, 2186–2198. [CrossRef]
7. Makar, G.L.; Kruger, J. Corrosion of magnesium. *Int. Mater. Rev.* **1993**, *38*, 138–153. [CrossRef]
8. Kendig, M.; Jeanjaquet, S.; Addison, R.; Waldrop, J. Role of hexavalent chromium in the inhibition of corrosion of aluminum alloys. *Surf. Coat. Technol.* **2001**, *140*, 58–66. [CrossRef]
9. Shahid, M.; Shamshad, S.; Rafiq, M.; Khalid, S.; Bibi, I.; Niazi, N.K.; Dumat, C.; Rashid, M.I. Chromium speciation, bioavailability, uptake, toxicity and detoxification in soil-plant system: A review. *Chemosphere* **2017**, *178*, 513–533. [CrossRef]
10. Carragher, U.; Breslin, C.B. Polypyrrole doped with dodecylbenzene sulfonate as a protective coating for copper. *Electrochim. Acta* **2018**, *291*, 362–372. [CrossRef]
11. Carragher, U.; Branagan, D.; Breslin, C.B. The influence of carbon nanotubes on the protective properties of polypyrrole formed at copper. *Materials* **2019**, *12*, 2587. [CrossRef]
12. Chong, K.Z.; Shih, T.S. Conversion-coating treatment for magnesium alloys by a permanganate-phosphate solution. *Mater. Chem. Phys.* **2003**, *80*, 191–200. [CrossRef]
13. Jiang, L.; Dong, Y.; Yuan, Y.; Zhou, X.; Liu, Y.; Meng, X. Recent advances of metal–organic frameworks in corrosion protection: From synthesis to applications. *Chem. Eng. J.* **2022**, *430*, 132823. [CrossRef]
14. Hayatgheib, Y.; Ramezanzadeh, B.; Kardar, P.; Mahdavian, M. A comparative study on fabrication of a highly effective corrosion protective system based on graphene oxide-polyaniline nanofibers/epoxy composite. *Corros. Sci.* **2018**, *133*, 358–373. [CrossRef]
15. Zhang, Y.; Zhao, M.; Zhang, J.; Shao, Q.; Li, J.; Li, H.; Lin, B.; Yu, M.; Chen, S.; Guo, Z. Excellent corrosion protection performance of epoxy composite coatings filled with silane functionalized silicon nitride. *J. Polym. Res.* **2018**, *25*, 130. [CrossRef]
16. Lei, W.; Zhou, T.; Pang, X.; Xue, S.; Xu, Q. Low-dimensional MXenes as noble metal-free co-catalyst for solar-to-fuel production: Progress and prospects. *J. Mater. Sci. Technol.* **2022**, *114*, 143–164. [CrossRef]
17. Wang, Y.; Li, S.; Zhang, D.; Tan, F.; Li, L.; Hu, G. Self-supported hierarchical P, Cu-codoped cobalt selenide nanoarrays for enhanced overall water splitting. *J. Alloys Compd.* **2022**, *889*, 161696. [CrossRef]
18. Goswami, P.; Gupta, G. Recent progress of flexible NO_2 and NH_3 gas sensors based on transition metal dichalcogenides for room temperature sensing. *Mater. Today Chem.* **2022**, *23*, 100726. [CrossRef]
19. Murali, A.; Lokhande, G.; Deo, K.A.; Brokesh, A.; Gaharwar, A.K. Emerging 2D nanomaterials for biomedical applications. *Mater. Today* **2021**, *50*, 276–302. [CrossRef]
20. Kirkland, N.T.; Schiller, T.; Medhekar, N.; Birbilis, N. Exploring graphene as a corrosion protection barrier. *Corros. Sci.* **2012**, *56*, 1–4. [CrossRef]
21. Healy, B.; Yu, T.; da Silva Alves, D.; Breslin, C.B. Review of recent developments in the formulation of graphene-based coatings for the corrosion protection of metals and alloys. *Corros. Mater. Degrad.* **2020**, *1*, 15. [CrossRef]
22. Schriver, M.; Regan, W.; Gannett, W.J.; Zaniewski, A.M.; Crommie, M.F.; Zettl, A. Graphene as a long-term metal oxidation barrier: Worse than nothing. *ACS Nano* **2013**, *7*, 5763–5768. [CrossRef] [PubMed]
23. Chauhan, D.S.; Quraishi, M.A.; Ansari, K.R.; Saleh, T.A. Graphene and graphene oxide as new class of materials for corrosion control and protection: Present status and future scenario. *Prog. Org. Coat.* **2020**, *147*, 105741. [CrossRef]
24. Kulyk, B.; Freitas, M.A.; Santos, N.F.; Mohseni, F.; Carvalho, A.F.; Yasakau, K.; Fernandes, A.J.S.; Bernardes, A.; Figueiredo, B.; Silva, R.; et al. A critical review on the production and application of graphene and graphene-based materials in anti-corrosion coatings. *Crit. Rev. Solid State Mater. Sci.* **2021**, 1–48. [CrossRef]
25. Ma, R.; Liu, Z.; Takada, K.; Iyi, N.; Bando, Y.; Sasaki, T. Synthesis and exfoliation of Co^{2+}-Fe^{3+} layered double hydroxides: An innovative topochemical approach. *J. Am. Chem. Soc.* **2007**, *129*, 5257–5263. [CrossRef]
26. Eng, A.Y.S.; Ambrosi, A.; Sofer, Z.; Šimek, P.; Pumera, M. Electrochemistry of transition metal dichalcogenides: Strong dependence on the metal-to-chalcogen composition and exfoliation method. *ACS Nano* **2014**, *8*, 12185–12198. [CrossRef]
27. Naguib, M.; Mashtalir, O.; Carle, J.; Presser, V.; Lu, J.; Hultman, L.; Gogotsi, Y.; Barsoum, M.W. Two-dimensional transition metal carbides. *ACS Nano* **2012**, *6*, 1322–1331. [CrossRef]

28. Gao, R.; Yin, L.; Wang, C.; Qi, Y.; Lun, N.; Zhang, L.; Liu, Y.-X.; Kang, L.; Wang, X. High-yield synthesis of boron nitride nanosheets with strong ultraviolet. *J. Phys. Chem. C* **2009**, *113*, 15160–15165. [CrossRef]

29. Dong, F.; Wang, Z.; Sun, Y.; Ho, W.-K.; Zhang, H. Engineering the nanoarchitecture and texture of polymeric carbon nitride semiconductor for enhanced visible light photocatalytic activity. *J. Colloid Interface Sci.* **2013**, *401*, 70–79. [CrossRef]

30. Wang, Q.; Ohare, D. Recent advances in the synthesis and application of layered double hydroxide (LDH) nanosheets. *Chem. Rev.* **2012**, *112*, 4124–4155. [CrossRef]

31. Zheludkevich, M.L.; Poznyak, S.K.; Rodrigues, L.M.; Raps, D.; Hack, T.; Dick, L.F.; Nunes, T.; Ferreira, M.G.S. Active protection coatings with layered double hydroxide nanocontainers of corrosion inhibitor. *Corros. Sci.* **2010**, *52*, 602–611. [CrossRef]

32. Manzeli, S.; Ovchinnikov, D.; Pasquier, D.; Yazyev, O.V.; Kis, A. 2D transition metal dichalcogenides. *Nat. Rev. Mater.* **2017**, *2*, 17033. [CrossRef]

33. Acerce, M.; Voiry, D.; Chhowalla, M. Metallic 1T phase MoS_2 nanosheets as supercapacitor electrode materials. *Nat. Nanotechnol.* **2015**, *10*, 313–318. [CrossRef]

34. Zhang, W.; Zhang, P.; Su, Z.; Wei, G. Synthesis and sensor applications of MoS_2-based nanocomposites. *Nanoscale* **2015**, *7*, 18364–18378. [CrossRef] [PubMed]

35. Anasori, B.; Lukatskaya, M.R.; Gogotsi, Y. 2D metal carbides and nitrides (MXenes) for energy storage. *Nat. Rev. Mater.* **2017**, *2*, 16098. [CrossRef]

36. Naguib, M.; Mochalin, V.N.; Barsoum, M.W.; Gogotsi, Y. 25th anniversary article: MXenes: A new family of two-dimensional materials. *Adv. Mater.* **2014**, *26*, 992–1005. [CrossRef] [PubMed]

37. Lukatskaya, M.R.; Halim, J.; Dyatkin, B.; Naguib, M.; Buranova, Y.S.; Barsoum, M.W.; Gogotsi, Y. Room-temperature carbide-derived carbon synthesis by electrochemical etching of MAX phases. *Angew. Chem. Int. Ed.* **2014**, *53*, 4877–4880. [CrossRef]

38. Niu, P.; Zhang, L.; Liu, G.; Cheng, H.-M. Graphene-like carbon nitride nanosheets for improved photocatalytic activities. *Adv. Funct. Mater.* **2012**, *22*, 4763–4770. [CrossRef]

39. Zhang, K.; Feng, Y.; Wang, F.; Yang, Z.; Wang, J. Two dimensional hexagonal boron nitride (2D-hBN): Synthesis, properties and applications. *J. Mater. Chem. C* **2017**, *5*, 11992–12022. [CrossRef]

40. Chen, T.-A.; Chuu, C.-P.; Tseng, C.-C.; Wen, C.-K.; Wong, H.-S.P.; Pan, S.; Li, R.; Chao, T.-A.; Chueh, W.-C.; Zhang, Y.; et al. Wafer-scale single-crystal hexagonal boron nitride monolayers on Cu (111). *Nature* **2020**, *579*, 219–223. [CrossRef]

41. Thomas, A.; Fischer, A.; Goettmann, F.; Antonietti, M.; Müller, J.-O.; Schlögl, R.; Carlsson, J.M. Graphitic carbon nitride materials: Variation of structure and morphology and their use as metal-free catalysts. *J. Mater. Chem.* **2008**, *18*, 4893–4908. [CrossRef]

42. Fina, F.; Callear, S.K.; Carins, G.M.; Irvine, J.T.S. Structural investigation of graphitic carbon nitride via XRD and neutron diffraction. *Chem. Mater.* **2015**, *27*, 2612–2618. [CrossRef]

43. Mounet, N.; Gibertini, M.; Schwaller, P.; Campi, D.; Merkys, A.; Marrazzo, A.; Sohier, T.; Castelli, I.E.; Cepellotti, A.; Pizzi, G.; et al. Two-dimensional materials from high-throughput computational exfoliation of experimentally known compounds. *Nat. Nanotechnol.* **2018**, *13*, 246–252. [CrossRef] [PubMed]

44. Schwinghammer, K.; Mesch, M.B.; Duppel, V.; Ziegler, C.; Senker, J.; Lotsch, B.V. Crystalline carbon nitride nanosheets for improved visible-light hydrogen evolution. *J. Am. Chem. Soc.* **2014**, *136*, 1730–1733. [CrossRef]

45. Cai, Z.; Liu, B.; Zou, X.; Cheng, H.-M. Chemical vapor deposition growth and applications of two-dimensional materials and their heterostructures. *Chem. Rev.* **2018**, *118*, 6091–6133. [CrossRef]

46. Shi, Y.; Li, H.; Li, L.-J. Recent advances in controlled synthesis of two-dimensional transition metal dichalcogenides via vapour deposition techniques. *Chem. Soc. Rev.* **2015**, *44*, 2744–2756. [CrossRef]

47. Ramki, S.; Sukanya, R.; Chen, S.-M.; Sakthivel, M.; Wang, J.Y. Simple hydrothermal synthesis of defective $CeMoSe_2$ dendrites as an effective electrocatalyst for the electrochemical sensing of 4-nitrophenol in water samples. *New J. Chem.* **2019**, *43*, 17200–17210. [CrossRef]

48. Gholami, P.; Dinpazhoh, L.; Khataee, A.; Hassani, A.; Bhatnagar, A. Facile hydrothermal synthesis of novel Fe-Cu layered double hydroxide/biochar nanocomposite with enhanced sonocatalytic activity for degradation of cefazolin sodium. *J. Hazard. Mater.* **2020**, *381*, 120742. [CrossRef]

49. Zheng, Y.; Liu, J.; Liang, J.; Jaroniec, M.; Qiao, S.Z. Graphitic carbon nitride materials: Controllable synthesis and applications in fuel cells and photocatalysis. *Energy Environ. Sci.* **2012**, *5*, 6717–6731. [CrossRef]

50. Kubota, Y.; Watanabe, K.; Tsuda, O.; Taniguchi, T. Deep ultraviolet light-emitting hexagonal boron nitride synthesized at atmospheric pressure. *Science* **2007**, *317*, 932–934. [CrossRef]

51. Taniguchi, T.; Watanabe, K. Synthesis of high-purity boron nitride single crystals under high pressure by using Ba-BN solvent. *J. Cryst. Growth* **2007**, *303*, 525–529. [CrossRef]

52. Tian, Z.; Wu, F.; Hu, P.; Ding, J.; Zhang, Y.; Zhang, P.; Sun, Z. Synthesis of $Ti_3(Sn_xAl_{1-x})C_2$ solid solutions over the whole composition range. *J. Alloys Compd.* **2022**, *894*, 162429. [CrossRef]

53. Mahmoudabadi, Z.S.; Rashidi, A.; Tavasoli, A.; Esrafili, M.; Panahi, M.; Askarieh, M.; Khodabakhshi, S. Ultrasonication-assisted synthesis of 2D porous MoS_2/GO nanocomposite catalysts as high-performance hydrodesulfurization catalysts of vacuum gasoil: Experimental and DFT study. *Ultrason. Sonochem.* **2021**, *74*, 105558. [CrossRef] [PubMed]

54. Zeng, Z.; Yin, Z.; Huang, X.; Li, H.; He, Q.; Lu, G.; Boey, F.; Zhang, H. Single-layer semiconducting nanosheets: High-yield preparation and device fabrication. *Angew. Chem. Int. Ed.* **2011**, *50*, 11093–11097. [CrossRef]

55. Yang, D.; Frindt, R.F. Li-intercalation and exfoliation of WS_2. *J. Phys. Chem. Solids* **1996**, *57*, 1113–1116. [CrossRef]

56. Zhang, M.; Yang, Y.; An, X.; Zhao, J.; Bao, Y.; Hou, L.-A. Exfoliation method matters: The microstructure-dependent photoactivity of g-C$_3$N$_4$ nanosheets for water purification. *J. Hazard. Mater.* **2022**, *424*, 127424. [CrossRef]

57. Meziani, M.J.; Sheriff, K.; Parajuli, P.; Priego, P.; Bhattacharya, S.; Rao, A.M.; Quimby, J.L.; Qiao, R.; Wang, P.; Hwu, S.-J.; et al. Advances in studies of boron nitride nanosheets and nanocomposites for thermal transport and related applications. *ChemPhysChem* **2022**, *23*. [CrossRef]

58. Cui, M.; Ren, S.; Qin, S.; Xue, Q.; Zhao, H.; Wang, L. Processable poly(2-butylaniline)/hexagonal boron nitride nanohybrids for synergetic anticorrosive reinforcement of epoxy coating. *Corros. Sci.* **2018**, *131*, 187–198. [CrossRef]

59. Vazirinasab, E.; Jafari, R.; Momen, G. Application of superhydrophobic coatings as a corrosion barrier: A review. *Surf. Coat. Technol.* **2018**, *341*, 40–56. [CrossRef]

60. Olajire, A.A. Recent advances on organic coating system technologies for corrosion protection of offshore metallic structures. *J. Mol. Liq.* **2018**, *269*, 572–606. [CrossRef]

61. Lyon, S.B.; Bingham, R.; Mills, D.J. Advances in corrosion protection by organic coatings: What we know and what we would like to know. *Prog. Org. Coat.* **2017**, *102*, 2–7. [CrossRef]

62. Zheng, B.; Ou, J.; Li, H.; Zhou, Z.; Qin, A.; Zhang, K.; Wang, X. Preparation of phosphate ion-doped Zn–Fe-layered double hydroxide with corrosion resistance and inducing Ca–P deposition on AZ31 Mg alloy. *J. Mater. Res.* **2022**, 1–10. [CrossRef]

63. Anjum, M.J.; Zhao, J.-M.; Asl, V.Z.; Malik, M.U.; Yasin, G.; Khan, W.Q. Green corrosion inhibitors intercalated Mg:Al layered double hydroxide coatings to protect Mg alloy. *Rare Met.* **2021**, *40*, 2254–2265. [CrossRef]

64. Haddadi, S.A.; Hu, S.; Ghaderi, S.; Ghanbari, A.; Ahmadipour, M.; Pung, S.-Y.; Li, S.; Feilizadeh, M.; Arjmand, M. Amino-functionalized MXene nanosheets doped with Ce(III) as potent nanocontainers toward self-healing epoxy nanocomposite coating for corrosion protection of mild steel. *ACS Appl. Mater. Interfaces* **2021**, *13*, 42074–42093. [CrossRef] [PubMed]

65. Stern, M.; Geary, A.L. Electrochemical polarization: I. A theoretical analysis of the shape of polarization curves. *J. Electrochem. Soc.* **1957**, *104*, 56–63. [CrossRef]

66. Aziz-Kerrzo, M.; Conroy, K.G.; Fenelon, A.M.; Farrell, S.T.; Breslin, C.B. Electrochemical studies on the stability and corrosion resistance of titanium-based implant materials. *Biomaterials* **2001**, *22*, 1531–1539. [CrossRef]

67. Grundmeier, G.; Schmidt, W.; Stratmann, M. Corrosion protection by organic coatings: Electrochemical mechanism and novel methods of investigation. *Electrochim. Acta* **2000**, *45*, 2515–2533. [CrossRef]

68. Tarzanagh, Y.J.; Seifzadeh, D.; Samadianfard, R. Combining the 8-hydroxyquinoline intercalated layered double hydroxide film and sol—gel coating for active corrosion protection of the magnesium alloy. *Int. J. Miner. Metall. Mater.* **2022**, *29*, 536–546. [CrossRef]

69. Yao, W.; Chen, Y.; Wu, L.; Zhang, J.; Pan, F. Effective corrosion and wear protection of slippery liquid-infused porous surface on AZ31 Mg alloy. *Surf. Coat. Technol.* **2022**, *429*, 127953. [CrossRef]

70. Ardelean, H.; Frateur, I.; Marcus, P. Corrosion protection of magnesium alloys by cerium, zirconium and niobium-based conversion coatings. *Corros. Sci.* **2008**, *50*, 1907–1918. [CrossRef]

71. Huang, M.; Zhang, H.; Yang, J. Synthesis of organic silane microcapsules for self-healing corrosion resistant polymer coatings. *Corros. Sci.* **2012**, *65*, 561–566. [CrossRef]

72. Yan, H.; Li, W.; Li, H.; Fan, X.; Zhu, M. Ti$_3$C$_2$ MXene nanosheets toward high-performance corrosion inhibitor for epoxy coating. *Prog. Org. Coat.* **2019**, *135*, 156–167. [CrossRef]

73. Zhang, D.; Peng, F.; Tan, J.; Liu, X. In-situ growth of layered double hydroxide films on biomedical magnesium alloy by transforming metal oxyhydroxide. *Appl. Surf. Sci.* **2019**, 143690. [CrossRef]

74. Ma, X.; Ma, Z.; Lu, D.; Jiang, Q.; Li, L.; Liao, T.; Hou, B. Enhanced photoelectrochemical cathodic protection performance of MoS$_2$/TiO$_2$ nanocomposites for 304 stainless steel under visible light. *J. Mater. Sci. Technol.* **2021**, *64*, 21–28. [CrossRef]

75. Zheng, H.; Sun, X.; Liu, Y.; Jiang, S.; Wang, D.; Fan, Y.; Hu, L.; Zhang, D.; Yao, W.; Zhang, L. New g-C$_3$N$_4$/GO/MoS$_2$ composites as efficient photocatalyst for photocathodic protection of 304 stainless steel. *Water Sci. Technol.* **2021**, *84*, 499–511. [CrossRef]

76. Husain, E.; Narayanan, T.N.; Taha-Tijerina, J.J.; Vinod, S.; Vajtai, R.; Ajayan, P.M. Marine corrosion protective coatings of hexagonal boron nitride thin films on stainless steel. *ACS Appl. Mater. Interfaces* **2013**, *5*, 4129–4135. [CrossRef]

77. Zuo, J.; Wu, B.; Luo, C.; Dong, B.; Xing, F. Preparation of MgAl layered double hydroxides intercalated with nitrite ions and corrosion protection of steel bars in simulated carbonated concrete pore solution. *Corros. Sci.* **2019**, *152*, 120–129. [CrossRef]

78. Jiang, H.; Wang, Z.; Ma, L.; Yang, Q.; Tang, Z.; Song, X.; Zeng, H.; Zhi, C. Boron ink assisted in situ boron nitride coatings for anti-oxidation and anti-corrosion applications. *Nanotechnology* **2019**, *30*, 335704. [CrossRef]

79. Zhang, F.; Sun, M.; Xu, S.; Zhao, L.; Zhang, B. Fabrication of oriented layered double hydroxide films by spin coating and their use in corrosion protection. *Chem. Eng. J.* **2008**, *141*, 362–367. [CrossRef]

80. Hou, L.; Li, Y.; Sun, J.; Zhang, S.H.; Wei, H.; Wei, Y. Enhancement corrosion resistance of Mg–Al layered double hydroxides films by anion-exchange mechanism on magnesium alloys. *Appl. Surf. Sci.* **2019**, *487*, 101–108. [CrossRef]

81. Wang, F.; Guo, Z. Facile synthesis of superhydrophobic three-metal-component layered double hydroxide films on aluminum foils for highly improved corrosion inhibition. *New J. Chem.* **2019**, *43*, 2289–2298. [CrossRef]

82. Iqbal, M.A.; Fedel, M. Effect of synthesis conditions on the controlled growth of MgAl-LDH corrosion resistance film: Structure and corrosion resistance properties. *Coatings* **2019**, *9*, 30. [CrossRef]

83. Wang, J.; Li, D.; Yu, X.; Jing, X.; Zhang, M.; Jiang, Z. Hydrotalcite conversion coating on Mg alloy and its corrosion resistance. *J. Alloys Compd.* **2010**, *494*, 271–274. [CrossRef]

84. Yan, L.; Zhou, M.; Pang, X.; Gao, K. One-step in situ synthesis of reduced graphene oxide/Zn-Al layered double hydroxide film for enhanced corrosion protection of magnesium alloys. *Langmuir* **2019**, *35*, 6312–6320. [CrossRef]

85. Zhong, F.; He, Y.; Wang, P.; Chen, C.; Xie, P.; Li, H.; Chen, J. One-step hydrothermal synthesis of reduced graphene oxide/aspartic acid intercalated layered double hydroxide for enhancing barrier and self-healing properties of epoxy coating. *React. Funct. Polym.* **2019**, *145*, 104380. [CrossRef]

86. Song, Y.; Tang, Y.; Fang, L.; Wu, F.; Zeng, X.; Hu, J.; Zhang, S.F.; Jiang, B.; Luo, H. Enhancement of corrosion resistance of AZ31 Mg alloys by one-step in situ synthesis of ZnAl-LDH films intercalated with organic anions (ASP, La). *J. Magnes. Alloy.* **2021**, *9*, 658–667. [CrossRef]

87. Pushparaj, S.S.C.; Forano, C.; Prevot, V.; Lipton, A.S.; Rees, G.J.; Hanna, J.V.; Nielsen, U.G. How the method of synthesis governs the local and global structure of zinc aluminum layered double hydroxides. *J. Phys. Chem. C* **2015**, *119*, 27695–27707. [CrossRef]

88. Guo, X.; Zhang, F.; Evans, D.G.; Duan, X. Layered double hydroxide films: Synthesis, properties and applications. *Chem. Commun.* **2010**, *46*, 5197–5210. [CrossRef]

89. Ji, G.; Prakash, R. Hydrothermal synthesis of Zn-Mg-based layered double hydroxide coatings for the corrosion protection of copper in chloride and hydroxide media. *Int. J. Miner. Metall. Mater.* **2021**, *28*, 1991–2000. [CrossRef]

90. Ma, L.; Qiang, Y.; Zhao, W. Designing novel organic inhibitor loaded MgAl-LDHs nanocontainer for enhanced corrosion resistance. *Chem. Eng. J.* **2021**, *408*, 127367. [CrossRef]

91. Lei, X.; Wang, L.; Zhao, X.; Chang, Z.; Jiang, M.; Yan, D.; Sun, X. Oriented CuZnAl ternary layered double hydroxide films: In situ hydrothermal growth and anticorrosion properties. *Ind. Eng. Chem. Res.* **2013**, *52*, 17934–17940. [CrossRef]

92. Vieira, D.E.L.; Sokol, D.; Smalenskaite, A.; Kareiva, A.; Ferreira, M.G.S.; Vieira, J.M.; Salak, A.N. Cast iron corrosion protection with chemically modified Mg—Al layered double hydroxides synthesized using a novel approach. *Surf. Coat. Technol.* **2019**, *375*, 158–163. [CrossRef]

93. Yan, H.; Wang, J.; Zhang, Y.; Hu, W. Preparation and inhibition properties of molybdate intercalated ZnAlCe layered double hydroxide. *J. Alloys Compd.* **2016**, *678*, 171–178. [CrossRef]

94. Zuo, J.-D.; Peng, Z.-C.; Dong, B.-Q.; Wang, Y.-S. In situ growth of corrosion resistant Mg-Fe layered double hydroxide film on Q235 steel. *J. Colloid Interface Sci.* **2022**, *610*, 202–212. [CrossRef] [PubMed]

95. Iqbal, M.A.; Fedel, M. Effect of operating parameters on the structural growth of ZnAl layered double hydroxide on AA6082 and corresponding corrosion resistance properties. *J. Coat. Technol. Res.* **2019**, *16*, 1423–1433. [CrossRef]

96. Serdechnova, M.; Salak, A.N.; Barbosa, F.S.; Vieira, D.E.L.; Tedim, J.; Zheludkevich, M.L.; Ferreira, M.G.S. Interlayer intercalation and arrangement of 2-mercaptobenzothiazolate and 1,2,3-benzotriazolate anions in layered double hydroxides: In situ X-ray diffraction study. *J. Solid State Chem.* **2016**, *233*, 158–165. [CrossRef]

97. Tedim, J.; Poznyak, S.K.; Kuznetsova, A.; Raps, D.; Hack, T.; Zheludkevich, M.L.; Ferreira, M.G.S. Enhancement of active corrosion protection via combination of inhibitor-loaded nanocontainers. *ACS Appl. Mater. Interfaces* **2010**, *2*, 1528–1535. [CrossRef]

98. Poznyak, S.K.; Tedim, J.; Rodrigues, L.M.; Salak, A.N.; Zheludkevich, M.L.; Dick, L.F.P.; Ferreira, M.G.S. Novel inorganic host layered double hydroxides intercalated with guest organic inhibitors for anticorrosion applications. *ACS Appl. Mater. Interfaces* **2009**, *1*, 2353–2362. [CrossRef]

99. Montemor, M.F.; Snihirova, D.V.; Taryba, M.G.; Lamaka, S.V.; Kartsonakis, I.A.; Balaskas, A.C.; Kordas, G.C.; Tedim, J.; Kuznetsova, A.; Zheludkevich, M.L.; et al. Evaluation of self-healing ability in protective coatings modified with combinations of layered double hydroxides and cerium molibdate nanocontainers filled with corrosion inhibitors. *Electrochim. Acta* **2012**, *60*, 31–40. [CrossRef]

100. Xie, P.; He, Y.; Zhong, F.; Zhang, C.; Chen, C.; Li, H.; Liu, Y.; Bai, Y.; Chen, J. Cu-BTA complexes coated layered double hydroxide for controlled release of corrosion inhibitors in dual self-healing waterborne epoxy coatings. *Prog. Org. Coat.* **2021**, *153*, 106164. [CrossRef]

101. Imanieh, I.; Afshar, A. Corrosion protection of aluminum by smart coatings containing layered double hydroxide (LDH) nanocontainers. *J. Mater. Res. Technol.* **2019**, *8*, 3004–3023. [CrossRef]

102. Chhetri, S.; Samanta, P.; Murmu, N.C.; Kuila, T. Anticorrosion properties of epoxy composite coating reinforced by molybdate-intercalated functionalized layered double hydroxide. *J. Compos. Sci.* **2019**, *3*, 11. [CrossRef]

103. Shkirskiy, V.; Keil, P.; Hintze-Bruening, H.; Leroux, F.; Vialat, P.; Lefèvre, G.; Ogle, K.; Volovitch, P. Factors affecting MoO_4^{2-} inhibitor release from Zn2Al based layered double hydroxide and their implication in protecting hot dip galvanized steel by means of organic coatings. *ACS Appl. Mater. Interfaces* **2015**, *7*, 25180–25192. [CrossRef]

104. del Olmo, R.; Mohedano, M.; Matykina, E.; Arrabal, R. Permanganate loaded Ca-Al-LDH coating for active corrosion protection of 2024-T3 alloy. *Corros. Sci.* **2022**, *198*, 110144. [CrossRef]

105. Zhou, P.; Xu, J.; Yu, L. Inhibitive effect of $SiO_2@NO_2^-$ intercalated MgAl-LDH nanocomposite on steel in Cl^- contaminated saturated $Ca(OH)_2$ solution. *Corros. Sci.* **2022**, *195*, 109997. [CrossRef]

106. Cao, Y.; Zheng, D.; Lin, C. Effect of physical barrier and anion-exchange process of nitrate-intercalated ZnAl layered double hydroxide films grown on Al on corrosion protection. *Surf. Coat. Technol.* **2021**, *421*, 127436. [CrossRef]

107. Jiang, D.; Xia, X.; Hou, J.; Cai, G.; Zhang, X.; Dong, Z. A novel coating system with self-reparable slippery surface and active corrosion inhibition for reliable protection of Mg alloy. *Chem. Eng. J.* **2019**, *373*, 285–297. [CrossRef]

108. Tian, Y.; Wen, C.; Wang, G.; Deng, P.; Mo, W. Inhibiting property of nitrite intercalated layered double hydroxide for steel reinforcement in contaminated concrete condition. *J. Appl. Electrochem.* **2020**, *50*, 835–849. [CrossRef]

109. Su, Y.; Qiu, S.; Yang, D.; Liu, S.; Zhao, H.; Wang, L.; Xue, Q. Active anti-corrosion of epoxy coating by nitrite ions intercalated MgAl LDH. *J. Hazard. Mater.* **2020**, *391*, 122215. [CrossRef]

110. Wen, T.; Yan, R.; Wang, N.; Li, Y.; Chen, T.; Ma, H. PPA-containing layered double hydroxide (LDH) films for corrosion protection of a magnesium alloy. *Surf. Coat. Technol.* **2020**, *383*, 125255. [CrossRef]

111. Pancrecious, J.K.; Vineetha, S.V.; Bill, U.S.; Gowd, E.B.; Rajan, T.P.D. Ni–Al polyvanadate layered double hydroxide with nanoceria decoration for enhanced corrosion protection of aluminium alloy. *Appl. Clay Sci.* **2021**, *211*, 106199. [CrossRef]

112. Cao, Y.; Jin, S.; Zheng, D.; Lin, C. Facile fabrication of ZnAl layered double hydroxide film co-intercalated with vanadates and laurates by one-step post modification. *Colloids Interface Sci. Commun.* **2021**, *40*, 100351. [CrossRef]

113. Cao, Y.; Zheng, D.; Luo, J.; Zhang, F.; Wang, C.; Dong, S.; Ma, Y.; Liang, Z.; Lin, C. Enhanced corrosion protection by Al surface immobilization of in-situ grown layered double hydroxide films co-intercalated with inhibitors and low surface energy species. *Corros. Sci.* **2020**, *164*, 108340. [CrossRef]

114. Rodriguez, J.; Bollen, E.; Nguyen, T.D.; Portier, A.; Paint, Y.; Olivier, M.-G. Incorporation of layered double hydroxides modified with benzotriazole into an epoxy resin for the corrosion protection of Zn-Mg coated steel. *Prog. Org. Coat.* **2020**, *149*, 105894. [CrossRef]

115. Lutz, A.; van den Berg, O.; Wielant, J.; De Graeve, I.; Terryn, H. A multiple-action self-healing coating. *Front. Mater.* **2016**, *2*, 73. [CrossRef]

116. Carneiro, J.; Caetano, A.F.; Kuznetsova, A.; Maia, F.; Salak, A.N.; Tedim, J.; Scharnagl, N.; Zheludkevich, M.L.; Ferreira, M.G.S. Polyelectrolyte-modified layered double hydroxide nanocontainers as vehicles for combined inhibitors. *RSC Adv.* **2015**, *5*, 39916–39929. [CrossRef]

117. Ouyang, Y.; Li, L.-X.; Xie, Z.-H.; Tang, L.; Wang, F.; Zhong, C.-J. A self-healing coating based on facile pH-responsive nanocontainers for corrosion protection of magnesium alloy. *J. Magnes. Alloys* **2020**. [CrossRef]

118. Li, L.-X.; Xie, Z.-H.; Fernandez, C.; Wu, L.; Cheng, D.; Jiang, X.-H.; Zhong, C.-J. Development of a thiophene derivative modified LDH coating for Mg alloy corrosion protection. *Electrochim. Acta* **2020**, *330*, 135186. [CrossRef]

119. Chen, J.; Fang, L.; Wu, F.; Xie, J.; Hu, J.; Jiang, B.; Luo, H. Corrosion resistance of a self-healing rose-like MgAl-LDH coating intercalated with aspartic acid on AZ31 Mg alloy. *Prog. Org. Coat.* **2019**, *136*, 105234. [CrossRef]

120. Anjum, M.J.; Zhao, J.; Zahedi Asl, V.; Yasin, G.; Wang, W.; Wei, S.; Zhao, Z.; Qamar Khan, W. In-situ intercalation of 8-hydroxyquinoline in Mg-Al LDH coating to improve the corrosion resistance of AZ31. *Corros. Sci.* **2019**, *157*, 1–10. [CrossRef]

121. Espinoza-Vázquez, A.; Rodríguez-Gómez, F.J.; Vergara-Arenas, B.I.; Lomas-Romero, L.; Angeles-Beltrán, D.; Negrón-Silva, G.E.; Morales-Serna, J.A. Synthesis of 1,2,3-triazoles in the presence of mixed Mg/Fe oxides and their evaluation as corrosion inhibitors of API 5L X70 steel submerged in HCl. *RSC Adv.* **2017**, *7*, 24736–24746. [CrossRef]

122. Stimpfling, T.; Vialat, P.; Hintze-Bruening, H.; Keil, P.; Shkirskiy, V.; Volovitch, P.; Ogle, K.; Leroux, F. Amino Acid interleaved layered double hydroxides as promising hybrid materials for AA2024 corrosion inhibition. *Eur. J. Inorg. Chem.* **2016**, *2016*, 2006–2016. [CrossRef]

123. Hang, T.T.X.; Truc, T.A.; Duong, N.T.; Pébre, N.; Olivier, M.-G. Layered double hydroxides as containers of inhibitors in organic coatings for corrosion protection of carbon steel. *Prog. Org. Coat.* **2012**, *74*, 343–348. [CrossRef]

124. Jiménez-López, B.A.; Leyva-Ramos, R.; Salazar-Rábago, J.J.; Jacobo-Azuara, A.; Aragón-Piña, A. Adsorption of selenium(IV) oxoanions on calcined layered double hydroxides of Mg-Al-CO$_3$ from aqueous solution. Effect of calcination and reconstruction of lamellar structure. *Environ. Nanotechnol. Monit. Manag.* **2021**, *16*, 100580. [CrossRef]

125. Tedim, J.; Kuznetsova, A.; Salak, A.N.; Montemor, F.; Snihirova, D.; Pilz, M.; Zheludkevich, M.L.; Ferreira, M.G.S. Zn-Al layered double hydroxides as chloride nanotraps in active protective coatings. *Corros. Sci.* **2012**, *55*, 1–4. [CrossRef]

126. del Olmo, R.; Mohedano, M.; Mingo, B.; Arrabal, R.; Matykina, E. LDH post-treatment of flash PEO coatings. *Coatings* **2019**, *9*, 354. [CrossRef]

127. Serdechnova, M.; Mohedano, M.; Kuznetsov, B.; Mendis, C.L.; Starykevich, M.; Karpushenkov, S.; Tedim, J.; Ferreira, M.G.S.; Blawert, C.; Zheludkevich, M.L. PEO coatings with active protection based on in-situ formed LDH-nanocontainers. *J. Electrochem. Soc.* **2017**, *164*, C36–C45. [CrossRef]

128. Bouali, A.C.; Straumal, E.A.; Serdechnova, M.; Wieland, D.C.F.; Starykevich, M.; Blawert, C.; Hammel, J.U.; Lermontov, S.A.; Ferreira, M.G.S.; Zheludkevich, M.L. Layered double hydroxide based active corrosion protective sealing of plasma electrolytic oxidation/sol-gel composite coating on AA2024. *Appl. Surf. Sci.* **2019**, *494*, 829–840. [CrossRef]

129. Peng, F.; Wang, D.; Zhang, D.; Yan, B.; Cao, H.; Qiao, Y.; Liu, X. PEO/Mg-Zn-Al LDH composite coating on Mg Alloy as a Zn/Mg ion-release platform with multifunctions: Enhanced corrosion resistance, osteogenic, and antibacterial activities. *ACS Biomater. Sci. Eng.* **2018**, *4*, 4112–4121. [CrossRef]

130. Peng, F.; Wang, D.; Tian, Y.; Cao, H.; Qiao, Y.; Liu, X. Sealing the pores of PEO coating with Mg-Al layered double hydroxide: Enhanced corrosion resistance, cytocompatibility and drug delivery ability. *Sci. Rep.* **2017**, *7*, 1–12. [CrossRef]

131. Zhang, G.; Wu, L.; Tang, A.; Ma, Y.; Song, G.-L.; Zheng, D.; Jiang, B.; Atrens, A.; Pan, F. Active corrosion protection by a smart coating based on a MgAl-layered double hydroxide on a cerium-modified plasma electrolytic oxidation coating on Mg alloy AZ31. *Corros. Sci.* **2018**, *139*, 370–382. [CrossRef]

132. Wu, L.; Yang, D.; Zhang, G.; Zhang, Z.; Zhang, S.; Tang, A.; Pan, F. Fabrication and characterization of Mg-M layered double hydroxide films on anodized magnesium alloy AZ31. *Appl. Surf. Sci.* **2018**, *431*, 177–186. [CrossRef]

133. Kaseem, M.; Ramachandraiah, K.; Hossain, S.; Dikici, B. A review on LDH-smart functionalization of anodic films of Mg alloys. *Nanomaterials* **2021**, *11*, 536. [CrossRef] [PubMed]

134. Zhang, G.; Jiang, E.; Wu, L.; Ma, W.; Yang, H.; Tang, A.; Pan, F. Corrosion protection properties of different inhibitors containing PEO/LDHs composite coating on magnesium alloy AZ31. *Sci. Rep.* **2021**, *11*, 2774. [CrossRef]

135. Li, Y.; Lu, X.; Serdechnova, M.; Blawert, C.; Zheludkevich, M.L.; Qian, K.; Zhang, T.; Wang, F. Incorporation of LDH nanocontainers into plasma electrolytic oxidation coatings on Mg alloy. *J. Magnes. Alloys* **2021**. [CrossRef]

136. Iqbal, M.A.; Secchi, M.; Iqbal, M.A.; Montagna, M.; Zanella, C.; Fedel, M. MgAl-LDH/graphene protective film: Insight into LDH-graphene interaction. *Surf. Coat. Technol.* **2020**, *401*, 126253. [CrossRef]

137. Luo, X.; Yuan, S.; Pan, X.; Zhang, C.; Du, S.; Liu, Y. Synthesis and enhanced corrosion protection performance of reduced graphene oxide nanosheet/ZnAl layered double hydroxide composite films by hydrothermal continuous flow method. *ACS Appl. Mater. Interfaces* **2017**, *9*, 18263–18275. [CrossRef]

138. Zhang, Y.; Yu, P.; Wang, J.; Li, Y.; Chen, F.; Wei, K.; Zuo, Y. LDHs/graphene film on aluminum alloys for active protection. *Appl. Surf. Sci.* **2018**, *433*, 927–933. [CrossRef]

139. Kaseem, M.; Ko, Y.G. A novel hybrid composite composed of albumin, WO3, and LDHs film for smart corrosion protection of Mg alloy. *Compos. Part B Eng.* **2021**, *204*, 108490. [CrossRef]

140. Kaseem, M.; Ko, Y.G. A novel composite system composed of zirconia and LDHs film grown on plasma electrolysis coating: Toward a stable smart coating. *Ultrason. Sonochem.* **2018**, *49*, 316–324. [CrossRef]

141. Wu, L.; Ding, X.; Zheng, Z.; Ma, Y.; Atrens, A.; Chen, X.; Xie, Z.; Sun, D.; Pan, F. Fabrication and characterization of an actively protective Mg–Al LDHs/Al$_2$O$_3$ composite coating on magnesium alloy AZ31. *Appl. Surf. Sci.* **2019**, *487*, 558–568. [CrossRef]

142. Song, Y.; Wang, H.; Liu, Q.; Li, G.; Wang, S.; Zhu, X. Sodium dodecyl sulfate (SDS) intercalated Mg–Al layered double hydroxides film to enhance the corrosion resistance of AZ31 magnesium alloy. *Surf. Coat. Technol.* **2021**, *422*, 127524. [CrossRef]

143. Chen, Y.; Wu, L.; Yao, W.; Chen, Y.; Zhong, Z.; Ci, W.; Wu, J.; Xie, Z.; Yuan, Y.; Pan, F. A self-healing corrosion protection coating with graphene oxide carrying 8-hydroxyquinoline doped in layered double hydroxide on a micro-arc oxidation coating. *Corros. Sci.* **2022**, *194*, 109941. [CrossRef]

144. Xu, T.; Zhao, Y.; Zhou, J.-H.; Hu, J.-M. Composite nanocontainers synthesized by in-situ growth of metal organic frameworks on layered double hydroxides having both passive and active protecting capabilities. *Prog. Org. Coat.* **2022**, *164*, 106695. [CrossRef]

145. Song, Z.; Xie, Z.; Ding, L.; Zhang, Y.; Hu, X. Preparation of corrosion-resistant MgAl-LDH/Ni composite coating on Mg alloy AZ31B. *Colloids Surf. A Physicochem. Eng. Asp.* **2022**, *632*, 127699. [CrossRef]

146. Wu, L.; Ding, X.; Zheng, Z.; Tang, A.; Zhang, G.; Atrens, A.; Pan, F. Doublely-doped Mg-Al-Ce-V$_2$O$_7^{4-}$ LDH composite film on magnesium alloy AZ31 for anticorrosion. *J. Mater. Sci. Technol.* **2021**, *64*, 66–72. [CrossRef]

147. Wu, Y.; Wu, L.; Zheludkevich, M.L.; Chen, Y.; Serdechnova, M.; Yao, W.; Blawert, C.; Atrens, A.; Pan, F. MgAl-V$_2$O$_7^{4-}$ LDHs/(PEI/MXene)10 composite film for magnesium alloy corrosion protection. *J. Mater. Sci. Technol.* **2021**, *91*, 28–39. [CrossRef]

148. Britto, R.J.; Benck, J.D.; Young, J.L.; Hahn, C.; Deutsch, T.G.; Jaramillo, T.F. Molybdenum disulfide as a protection layer and catalyst for gallium indium phosphide solar water splitting photocathodes. *J. Phys. Chem. Lett.* **2016**, *7*, 2044–2049. [CrossRef]

149. King, L.A.; Hellstern, T.R.; Park, J.; Sinclair, R.; Jaramillo, T.F. Highly stable molybdenum disulfide protected silicon photocathodes for photoelectrochemical water splitting. *ACS Appl. Mater. Interfaces* **2017**, *9*, 36792–36798. [CrossRef]

150. Pham, V.P.; Yeom, G.Y. Recent advances in doping of molybdenum disulfide: Industrial applications and future prospects. *Adv. Mater.* **2016**, *28*, 9024–9059. [CrossRef]

151. Ding, J.; Zhao, H.; Zhao, X.; Xu, B.; Yu, H. How semiconductor transition metal dichalcogenides replaced graphene for enhancing anticorrosion. *J. Mater. Chem. A* **2019**, *7*, 13511–13521. [CrossRef]

152. Prado, L.H.; Virtanen, S. Cu-MoS$_2$ superhydrophobic coating by composite electrodeposition. *Coatings* **2020**, *10*, 238. [CrossRef]

153. Hong, M.-S.; Park, Y.; Kim, J.G.; Kim, K. Effect of incorporating MoS$_2$ in organic coatings on the corrosion resistance of 316L stainless steel in a 3.5% NaCl solution. *Coatings* **2019**, *9*, 45. [CrossRef]

154. Zhao, X.; Zhang, B.; Jin, Z.; Chen, C.; Zhu, Q.; Hou, B. Epoxy coating modified by 2D MoS$_2$/SDBS: Fabrication, anticorrosion behaviour and inhibition mechanism. *RSC Adv.* **2016**, *6*, 97512–97522. [CrossRef]

155. ArunKumar, S.; Jegathish, V.; Soundharya, R.; JesyAlka, M.; Arul, C.; Sathyanarayanan, S.; Mayavan, S. Evaluating the performance of MoS$_2$ based materials for corrosion protection of mild steel in an aggressive chloride environment. *RSC Adv.* **2017**, *7*, 17332–17335. [CrossRef]

156. Tang, B.; Yu, Z.G.; Seng, H.L.; Zhang, N.; Liu, X.; Zhang, Y.-W.; Yang, W.; Gong, H. Simultaneous edge and electronic control of MoS$_2$ nanosheets through Fe doping for an efficient oxygen evolution reaction. *Nanoscale* **2018**, *10*, 20113–20119. [CrossRef]

157. Li, Z.; Wang, X.; Dong, X.; Hu, F.; Liu, S.; Zhang, M.; Yuan, T.; Yu, Y.; Kuang, Q.; Ren, Q.; et al. Creating high-performance bi-functional composite coatings on magnesium−8lithium alloy through electrochemical surface engineering with highly enhanced corrosion and wear protection. *J. Alloys Compd.* **2020**, *818*, 153341. [CrossRef]

158. Qu, Z.; Wang, L.; Tang, H.; Ye, H.; Li, M. Effect of Nano-SnS and Nano-MoS$_2$ on the corrosion protection performance of the polyvinylbutyral and zinc-rich polyvinylbutyral coatings. *Nanomaterials* **2019**, *9*, 956. [CrossRef]

159. Asan, A.; Asan, G.; Çelikkan, H. Investigation of the effects of MoS$_2$ doped (PANI and PPy) coatings on mild steel corrosion in alkaline medium. *Acta Phys. Pol. A* **2019**, *135*, 987–989. [CrossRef]

160. Asan, G.; Asan, A.; Çelikkan, H. The effect of 2D-MoS$_2$ doped polypyrrole coatings on brass corrosion. *J. Mol. Struct.* **2020**, *1203*, 127318. [CrossRef]

161. Guan, Z.-C.; Wang, H.-P.; Wang, X.; Hu, J.; Du, R.-G. Fabrication of heterostructured β-Bi$_2$O$_3$-TiO$_2$ nanotube array composite film for photoelectrochemical cathodic protection applications. *Corros. Sci.* **2018**, *136*, 60–69. [CrossRef]

162. Korupalli, C.; You, K.-L.; Getachew, G.; Rasal, A.S.; Dirersa, W.B.; Fahmi, M.Z.; Chang, J.-Y. Engineering the surface of Ti$_3$C$_2$ MXene nanosheets for high stability and multimodal anticancer therapy. *Pharmaceutics* **2022**, *14*, 304. [CrossRef] [PubMed]

163. Soleymaniha, M.; Shahbazi, M.-A.; Rafieerad, A.R.; Maleki, A.; Amiri, A. Promoting role of MXene nanosheets in biomedical sciences: Therapeutic and biosensing innovations. *Adv. Healthc. Mater.* **2019**, *8*, e1801137. [CrossRef] [PubMed]

164. Li, S.; Huang, H.; Chen, F.; He, X.; Ma, Y.; Zhang, L.; Sheng, X.; Chen, Y.; Shchukina, E.; Shchukin, D. Reinforced anticorrosion performance of waterborne epoxy coating with eco-friendly L-cysteine modified Ti$_3$C$_2$T$_x$ MXene nanosheets. *Prog. Org. Coat.* **2021**, *161*, 106478. [CrossRef]

165. He, X.; Li, S.; Shen, R.; Ma, Y.; Zhang, L.; Sheng, X.; Chen, Y.; Xie, D.; Huang, J. A high-performance waterborne polymeric composite coating with long-term anti-corrosive property based on phosphorylation of chitosan-functionalized Ti$_3$C$_2$T$_x$ MXene. *Adv. Compos. Hybrid Mater.* **2022**, 1–13. [CrossRef]

166. Yan, H.; Fan, X.; Cai, M.; Song, S.; Zhu, M. Amino-functionalized Ti$_3$C$_2$T$_x$ loading ZIF-8 nanocontainer@benzotriazole as multifunctional composite filler towards self-healing epoxy coating. *J. Colloid Interface Sci.* **2021**, *602*, 131–145. [CrossRef]

167. Nie, Y.; Huang, J.; Ma, S.; Li, Z.; Shi, Y.; Yang, X.; Fang, X.; Zeng, J.; Bi, P.; Qi, J.; et al. MXene-hybridized silane films for metal anticorrosion and antibacterial applications. *Appl. Surf. Sci.* **2020**, *527*, 146915. [CrossRef]

168. Cao, H.; Fang, M.; Jia, W.; Liu, X.; Xu, Q. Remarkable improvement of corrosion resistance of silane composite coating with Ti$_3$C$_2$T$_x$ MXene on copper. *Compos. Part B Eng.* **2022**, *228*, 109427. [CrossRef]

169. Ding, J.; Zhao, H.; Yu, H. Structure and performance insights in carbon dots-functionalized MXene-epoxy ultrathin anticorrosion coatings. *Chem. Eng. J.* **2022**, *430*, 132838. [CrossRef]

170. Shen, L.; Zhao, W.; Wang, K.; Xu, J. GO-Ti$_3$C$_2$ two-dimensional heterojunction nanomaterial for anticorrosion enhancement of epoxy zinc-rich coatings. *J. Hazard. Mater.* **2021**, *417*, 126048. [CrossRef]

171. Yan, H.; Zhang, L.; Li, H.; Fan, X.; Zhu, M. Towards high-performance additive of Ti$_3$C$_2$/graphene hybrid with a novel wrapping structure in epoxy coating. *Carbon N. Y.* **2020**, *157*, 217–233. [CrossRef]

172. Cai, M.; Fan, X.; Yan, H.; Li, Y.; Song, S.; Li, W.; Li, H.; Lu, Z.; Zhu, M. In situ assemble Ti$_3$C$_2$T$_x$ MXene@MgAl-LDH heterostructure towards anticorrosion and antiwear application. *Chem. Eng. J.* **2021**, *419*, 130050. [CrossRef]

173. Zhou, M.; Zhao, C.; Liu, P.; Yu, H. Adsorption behavior of Ti$_3$C$_2$T$_x$ with h-BN nanosheet and their application in waterborne epoxy anti-corrosion coating. *Appl. Surf. Sci.* **2022**, *586*, 152778. [CrossRef]

174. Cai, M.; Feng, P.; Yan, H.; Li, Y.; Song, S.; Li, W.; Li, H.; Fan, X.; Zhu, M. Hierarchical Ti$_3$C$_2$T$_x$@MoS$_2$ heterostructures: A first principles calculation and application in corrosion/wear protection. *J. Mater. Sci. Technol.* **2022**, *116*, 151–160. [CrossRef]

175. Li, C.; Xu, J.; Xu, Q.; Xue, G.; Yu, H.; Wang, X.; Lu, J.; Cui, G.; Gu, G. Synthesis of Ti$_3$C$_2$ MXene@PANI composites for excellent anticorrosion performance of waterborne epoxy coating. *Prog. Org. Coat.* **2022**, *165*, 106673. [CrossRef]

176. Zhao, H.; Ding, J.; Zhou, M.; Yu, H. Air-stable titanium carbide MXene nanosheets for corrosion protection. *ACS Appl. Nano Mater.* **2021**, *4*, 3075–3086. [CrossRef]

177. Cui, M.; Ren, S.; Qin, S.; Xue, Q.; Zhao, H.; Wang, L. Non-covalent functionalized hexagonal boron nitride nanoplatelets to improve corrosion and wear resistance of epoxy coatings. *RSC Adv.* **2017**, *7*, 44043–44053. [CrossRef]

178. Cui, M.; Ren, S.; Chen, J.; Liu, S.; Zhang, G.; Zhao, H.; Wang, L.; Xue, Q. Anticorrosive performance of waterborne epoxy coatings containing water-dispersible hexagonal boron nitride (h-BN) nanosheets. *Appl. Surf. Sci.* **2017**, *397*, 77–86. [CrossRef]

179. Zhao, H.; Ding, J.; Yu, H. Advanced bio-based UV-curable anticorrosive coatings reinforced by hBN. *ChemistrySelect* **2018**, *3*, 11277–11283. [CrossRef]

180. Du, Y.; Zhang, Y.; Zhang, R.; Lin, S. Synthesis of ultrathin functional boron nitride nanosheets and their application in anticorrosion. *ACS Appl. Nano Mater.* **2021**, *4*, 11088–11096. [CrossRef]

181. Wu, Y.; He, Y.; Chen, C.; Zhong, F.; Li, H.; Chen, J.; Zhou, T. Non-covalently functionalized boron nitride by graphene oxide for anticorrosive reinforcement of water-borne epoxy coating. *Colloids Surf. A Physicochem. Eng. Asp.* **2020**, *587*, 124337. [CrossRef]

182. Zhao, H.-R.; Ding, J.-H.; Yu, H.-B. Phosphorylated boron nitride nanosheets as highly effective barrier property enhancers. *Ind. Eng. Chem. Res.* **2018**, *57*, 14096–14105. [CrossRef]

183. Wu, Y.; Yu, J.; Zhao, W.; Wang, C.; Wu, B.; Lu, G. Investigating the anti-corrosion behaviors of the waterborne epoxy composite coatings with barrier and inhibition roles on mild steel. *Prog. Org. Coat.* **2019**, *133*, 8–18. [CrossRef]

184. Yu, J.; Zhao, W.; Liu, G.; Wu, Y.; Wang, D. Anti-corrosion mechanism of 2D nanosheet materials in waterborne epoxy coatings. *Surf. Topogr. Metrol. Prop.* **2018**, *6*, 034019. [CrossRef]

185. Wu, Y.; He, Y.; Zhou, T.; Chen, C.; Zhong, F.; Xia, Y.; Xie, P.; Zhang, C. Synergistic functionalization of h-BN by mechanical exfoliation and PEI chemical modification for enhancing the corrosion resistance of waterborne epoxy coating. *Prog. Org. Coat.* **2020**, *142*, 105541. [CrossRef]

186. Ysiwata-Rivera, A.P.; Hernández-Hernández, E.; Cadenas-Pliego, G.; Ávila-Orta, C.A.; González-Morones, P.; Velásquez-de Jesús, J.A.; Cuara-Díaz, E.; Gallardo-Vega, C.A.; Mata-Padilla, J.M. Effect of modified hexagonal boron nitride nanoparticles on the emulsion stability, viscosity and electrochemical behavior of nanostructured acrylic coatings for the corrosion protection of AISI 304 stainless steel. *Coatings* **2020**, *10*, 488. [CrossRef]

187. Zhao, H.; Ding, J.; Yu, H. The efficient exfoliation and dispersion of hBN nanoplatelets: Advanced application to waterborne anticorrosion coatings. *New J. Chem.* **2018**, *42*, 14433–14443. [CrossRef]

188. Huang, Y.-C.; Lo, T.-Y.; Chao, C.-G.; Whang, W.-T. Anti-corrosion characteristics of polyimide/h-boron nitride composite films with different polymer configurations. *Surf. Coat. Technol.* **2014**, *260*, 113–117. [CrossRef]

189. Wang, J.; Wang, N.; Liu, M.; Ge, C.; Hou, B.; Liu, G.; Sun, W.; Hu, Y.; Ning, Y. Hexagonal boron nitride/poly(vinyl butyral) composite coatings for corrosion protection of copper. *J. Mater. Sci. Technol.* **2022**, *96*, 103–112. [CrossRef]

190. Li, J.; Gan, L.; Liu, Y.; Mateti, S.; Lei, W.; Chen, Y.; Yang, J. Boron nitride nanosheets reinforced waterborne polyurethane coatings for improving corrosion resistance and antifriction properties. *Eur. Polym. J.* **2018**, *104*, 57–63. [CrossRef]

191. Tang, X.; Wang, H.; Liu, C.; Zhu, X.; Gao, W.; Yin, H. Direct growth of hexagonal boron nitride nanofilms on stainless steel for corrosion protection. *ACS Appl. Nano Mater.* **2021**, *4*, 12024–12033. [CrossRef]

192. Khan, M.H.; Jamali, S.S.; Lyalin, A.; Molino, P.J.; Jiang, L.; Liu, H.K.; Taketsugu, T.; Huang, Z. Atomically thin hexagonal boron nitride nanofilm for Cuprotection: The importance of film perfection. *Adv. Mater.* **2017**, *29*, 1603937. [CrossRef] [PubMed]

193. Zhang, C.; He, Y.; Li, F.; Di, H.; Zhang, L.; Zhan, Y. h-BN decorated with Fe_3O_4 nanoparticles through mussel-inspired chemistry of dopamine for reinforcing anticorrosion performance of epoxy coatings. *J. Alloys Compd.* **2016**, *685*, 743–751. [CrossRef]

194. Scardamaglia, M.; Boix, V.; D'Acunto, G.; Struzzi, C.; Reckinger, N.; Chen, X.; Shivayogimath, A.; Booth, T.; Knudsen, J. Comparative study of copper oxidation protection with graphene and hexagonal boron nitride. *Carbon N. Y.* **2021**, *171*, 610–617. [CrossRef]

195. Yang, X.; Zhang, R.; Pu, J.; He, Z.; Xiong, L. 2D graphene and h-BN layers application in protective coatings. *Corros. Rev.* **2021**, *39*, 93–107. [CrossRef]

196. Li, X.; Long, Y.; Ma, L.; Li, J.; Yin, J.; Guo, W. Coating performance of hexagonal boron nitride and graphene layers. *2D Mater.* **2021**, *8*, 034002. [CrossRef]

197. Galbiati, M.; Stoot, A.C.; Mackenzie, D.M.A.; Bøggild, P.; Camilli, L. Real-time oxide evolution of copper protected by graphene and boron nitride barriers. *Sci. Rep.* **2017**, *7*, 39770. [CrossRef]

198. Zhou, Z.; Ji, X.; Pourhashem, S.; Duan, J.; Hou, B. Investigating the effects of $g\text{-}C_3N_4$/graphene oxide nanohybrids on corrosion resistance of waterborne epoxy coatings. *Compos. Part A Appl. Sci. Manuf.* **2021**, *149*, 106568. [CrossRef]

199. Karimi, M.A.; Haji Aghaei, V.; Nezhadali, A.; Ajami, N. Investigation of copper corrosion in sodium chloride solution by using a new coating of polystyrene/$g\text{-}C_3N_4$. *J. Mater. Sci. Mater. Electron.* **2019**, *30*, 6300–6310. [CrossRef]

200. Xu, J.H.; Ye, S.; Ding, C.D.; Tan, L.H.; Fu, J.J. Autonomous self-healing supramolecular elastomer reinforced and toughened by graphitic carbon nitride nanosheets tailored for smart anticorrosion coating applications. *J. Mater. Chem. A* **2018**, *6*, 5887–5898. [CrossRef]

201. Xia, Y.; He, Y.; Chen, C.; Wu, Y.; Zhong, F.; Chen, J. Co-modification of polydopamine and KH560 on $g\text{-}C_3N_4$ nanosheets for enhancing the corrosion protection property of waterborne epoxy coating. *React. Funct. Polym.* **2020**, *146*, 104405. [CrossRef]

202. Yang, S.; Gong, Y.; Zhang, J.; Zhan, L.; Ma, L.; Fang, Z.; Vajtai, R.; Wang, X.; Ajayan, P.M. Exfoliated graphitic carbon nitride nanosheets as efficient catalysts for hydrogen evolution under visible light. *Adv. Mater.* **2013**, *25*, 2452–2456. [CrossRef] [PubMed]

203. Zuo, S.; Chen, Y.; Liu, W.; Yao, C.; Li, Y.; Ma, J.; Kong, Y.; Mao, H.; Li, Z.; Fu, Y. Polyaniline/$g\text{-}C_3N_4$ composites as novel media for anticorrosion coatings. *J. Coat. Technol. Res.* **2017**, *14*, 1307–1314. [CrossRef]

204. Sheng, C.; Cheng, L.; Chen, X.; Zhang, Y.; Guo, W. Synergistic effect of 2D/0D mixed graphitic carbon nitride/Fe_2O_3 on the excellent corrosion behavior of epoxy-based waterborne coatings. *Colloid Polym. Sci.* **2021**, *299*, 883–897. [CrossRef]

205. Kumar, A.M.; Khan, M.Y.; Suleiman, R.K.; Khan, A.; Dafalla, H. Promising graphitic carbon nitride/MoO_x nanocomposites: For surface protective performance of AA2024 alloys in marine environment. *Surf. Coat. Technol.* **2019**, *374*, 579–590. [CrossRef]

206. Steffi, A.P.; Balaji, R.; Prakash, N.; Rajesh, T.P.; Ethiraj, S.; Samuel, M.S.; Nadda, A.K.; Chandrasekar, N. Incorporation of SiO_2 functionalized gC_3N_4 sheets with TiO_2 nanoparticles to enhance the anticorrosion performance of metal specimens in aggressive Cl^- environment. *Chemosphere* **2022**, *290*, 133332. [CrossRef]

207. Pourhashem, S.; Rashidi, A.; Alaei, M.; Moradi, M.-A.; Maklavany, D.M. Developing a new method for synthesizing amine functionalized $g\text{-}C_3N_4$ nanosheets for application as anti-corrosion nanofiller in epoxy coatings. *SN Appl. Sci.* **2019**, *1*, 108. [CrossRef]

208. Cao, S.; Low, J.; Yu, J.; Jaroniec, M. Polymeric Photocatalysts based on graphitic carbon nitride. *Adv. Mater.* **2015**, *27*, 2150–2176. [CrossRef]

209. Zhang, X.; Chen, G.; Li, W.; Wu, D. Graphitic carbon nitride homojunction films for photocathodic protection of 316 stainless steel and Q235 carbon steel. *J. Electroanal. Chem.* **2020**, *857*, 113703. [CrossRef]

210. Ma, Y.; Wang, H.; Sun, L.; Liu, E.; Fei, G.; Fan, J.; Kang, Y.-M. Unidirectional electron transport from graphitic-C_3N_4 for novel remote and long-term photocatalytic anti-corrosion on Q235 carbon steel. *Chem. Eng. J.* **2022**, *429*, 132520. [CrossRef]

211. Bu, Y.; Chen, Z. Highly efficient photoelectrochemical anticorrosion performance of C_3N_4ZnO composite with quasi-shell-core structure on 304 stainless steel. *RSC Adv.* **2014**, *4*, 45397–45406. [CrossRef]

212. Sun, M.; Chen, Z.; Bu, Y. Enhanced photoelectrochemical cathodic protection performance of the $C_3N_4@In_2O_3$ nanocomposite with quasi-shell-core structure under visible light. *J. Alloys Compd.* **2015**, *618*, 734–741. [CrossRef]